Article

Current Biology

Reprogramming of endolysosomes for melanogenesis in BLOC-1-deficient melanocytes

Graphical abstract

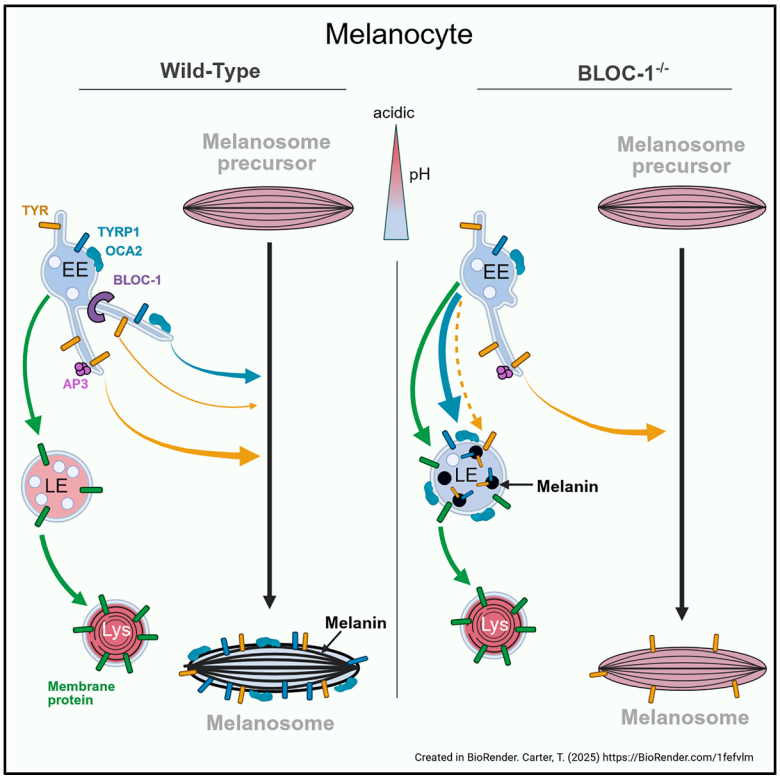

Highlights

- Melanin is formed in endolysosomal organelles in BLOC-1-deficient melanocytes
- cAMP-elevating agents increase melanin content of BLOC-1-deficient melanocytes
- OCA2 overexpression enhances BLOC-1-independent endolysosomal melanogenesis
- Endolysosomal pH neutralization dramatically enhances endolysosomal melanogenesis

Authors

Philip S. Goff, Shyamal Patel, Dawn C. Harper, Tom Carter, Michael S. Marks, Elena V. Sviderskaya

Correspondence

marksm@pennmedicine.upenn.edu (M.S. M.), esviders@citystgeorges.ac.uk (E.V.S.)

In brief

Proteins destined for melanosomes are mistargeted in part to endolysosomes in BLOC-1-deficient melanocytes. Goff et al. show that such cells reprogram endolysosomes to synthesize melanin pigments and that increasing melanogenic protein expression and/or organelle pH enhances endolysosomal melanogenesis in the absence of functional melanosomes.

Goff et al., 2025, Current Biology *35*, 1–17
August 4, 2025
https://doi.org/10.1016/j.cub.2025.06.031

CellPress

Please cite this article in press as: Goff et al., Reprogramming of endolysosomes for melanogenesis in BLOC-1-deficient melanocytes, Current Biology (2025), https://doi.org/10.1016/j.cub.2025.06.031

Current Biology

CellPress
OPEN ACCESS

Article

Reprogramming of endolysosomes for melanogenesis in BLOC-1-deficient melanocytes

Philip S. Goff,[1] Shyamal Patel,[1] Dawn C. Harper,[2] Tom Carter,[1] Michael S. Marks,[2,3,4,5,*] and Elena V. Sviderskaya[1,4,*]
[1]School of Health and Medical Sciences, City St. George's, University of London, Cranmer Terrace, London SW17 0RE, UK
[2]Department of Pathology & Laboratory Medicine, Children's Hospital of Philadelphia Research Institute, Philadelphia, PA 19104, USA
[3]Department of Pathology & Laboratory Medicine and Department of Physiology, Perelman School of Medicine, University of Pennsylvania, Philadelphia, PA 19104, USA
[4]These authors contributed equally
[5]Lead contact
*Correspondence: marksm@pennmedicine.upenn.edu (M.S.M.), esviders@citystgeorges.ac.uk (E.V.S.)
https://doi.org/10.1016/j.cub.2025.06.031

SUMMARY

Photoprotective melanins in the skin are synthesized by epidermal melanocytes within specialized lysosome-related organelles called melanosomes. Melanosomes coexist with lysosomes; thus, melanocytes employ trafficking machineries that possess cell-type-specific functions to ensure correct cargo delivery to either the endolysosomal system or maturing melanosomes. Mutations in some of the protein complexes required for melanogenic cargo delivery, such as biogenesis of lysosome-related organelles complex 1 (BLOC-1), result in hypopigmentation due to mistrafficking of cargo to endolysosomes. We show that hypopigmented BLOC-1-deficient melanocytes retain melanogenic capacity that can be enhanced by treatment with cyclic adenosine monophosphate (cAMP)-elevating agents despite the mislocalization of melanogenic proteins. The melanin formed in BLOC-1-deficient melanocytes is not generated in melanosomes but rather within late endosomes/lysosomes to which some cargoes mislocalize. Although these organelles generally are acidic, a cohort of late endosomes/lysosomes have a sufficiently neutral pH to facilitate melanogenesis, perhaps due to mislocalized melanosomal transporters and melanogenic enzymes. Modulation of the pH of late endosomes/lysosomes by genetic manipulation or via treatment with lysosomotropic agents significantly enhances the melanin content of BLOC-1-deficient melanocytes. Our data suggest that upregulated expression of mistargeted cargoes leads to both increased tyrosinase expression and subsequent activity due to pH modulation facilitating the reprogramming of a subset of endolysosomes to replicate some functions of lysosome-related organelles.

INTRODUCTION

Lysosome-related organelles (LROs) are a diverse group of tissue-specific organelles that share features and components with organelles of the endolysosomal system (reviewed by Bowman et al.[1]). One such LRO, the melanosome, is found within melanocytes, the melanin-producing cells that reside within the eye, hair follicles, and the basal layer of the epidermis within the skin. Melanin produced by epidermal melanocytes is transferred to surrounding keratinocytes, where it is arranged to form supranuclear caps that help protect against ultraviolet radiation.[2] Despite these photoprotective properties, melanin synthesis (melanogenesis) is an oxidative process that generates toxic intermediates.[3,4] Therefore, melanogenesis is confined within melanocytes to melanosomes likely as an adaptive response to protect against these potentially cytotoxic effects.[5]

Melanosomes mature through four morphologically distinct stages.[6] Stage I melanosomes are unpigmented acidic precursors that correspond to the vacuolar domains of early endosomes.[7] These organelles accumulate the pigment-cell-specific pre-melanosome protein (PMEL) and undergo significant remodeling to the characteristic ellipsoid shape associated with melanosomes to form unpigmented stage II melanosomes. This process is driven by the generation and elongation of amyloid fibrils formed following the proteolytic cleavage of PMEL.[8,9] Stage II melanosomes mature to partially pigmented stage III melanosomes and fully pigmented stage IV melanosomes, which, under physiological conditions, are transferred to surrounding epidermal keratinocytes or retained intracellularly within the eye.

The maturation from stage II to stage III melanosomes requires the coordinated delivery of proteins that facilitate melanogenesis. These include the melanogenic proteins tyrosinase (TYR), tyrosinase-related protein 1 (TYRP1), and dopachrome tautomerase (DCT), which are directly involved in the chemical synthesis of melanin. Accessory proteins are also required, such as ATP7A, which supplies the crucial melanogenic enzyme TYR with its cofactor, copper,[10] and ion channels and transporters (e.g., OCA2 and SLC45A2) that raise luminal pH[11,12] to near neutral and thus favor optimal TYR activity.[13,14] The expression of most of these melanogenic proteins is regulated by melanocortin-1 receptor (MC1R) signaling. MC1R is a G

Please cite this article in press as: Goff et al., Reprogramming of endolysosomes for melanogenesis in BLOC-1-deficient melanocytes, Current Biology (2025), https://doi.org/10.1016/j.cub.2025.06.031

protein-coupled receptor (GPCR) that, once bound by its physiological agonist, α-melanocyte-stimulating hormone (α-MSH), increases melanogenic protein expression and melanogenesis via a cyclic adenosine monophosphate (cAMP)-dependent pathway.[15–17] As such, numerous studies have focused on activating the MC1R pathway to increase photoprotective melanin.[18–22]

Several LROs, including melanosomes, coexist with conventional endolysosomal organelles in their respective cell types.[7] Therefore, cells that harbor LROs (including melanocytes) have specialized trafficking mechanisms to distinguish between endolysosomal cargoes and those that are destined for maturing LROs. Genetic disorders that disrupt these mechanisms affect the biogenesis and/or function of these organelles and underlie multiple systemic consequences. One group of such disorders is the Hermansky-Pudlak syndromes (HPS), syndromic disorders characterized minimally by oculocutaneous albinism and bleeding diathesis.[23] To date, 11 subtypes of HPS have been identified (HPS-1 to -11), each caused by mutations in a different gene.[24–33] The HPS genes encode specific subunits of four distinct obligate protein complexes—adaptor protein-3 (AP-3) and biogenesis of lysosome-related organelles complex-1, -2, and -3 (BLOC-1, -2, and -3)—that facilitate the delivery of cargoes to and from maturing LROs, including melanosomes. Loss of function of any subunit of one of these complexes destabilizes the other subunits of that complex.

The delivery of newly synthesized resident melanosomal proteins to maturing melanosomes is predominantly via early endosomes, facilitated in part by the HPS proteins. Disruption of any of the HPS complexes therefore impedes the delivery of specific melanogenic cargoes to melanosomes, resulting in a variable hypopigmentation phenotype. The majority of known melanogenic cargoes require BLOC-1 for exit from early endosomes toward maturing melanosomes.[10,34–36] BLOC-1 is a ubiquitously expressed protein complex composed of eight subunits[28,37–41] that form a flexible linear chain.[42] BLOC-1 facilitates cargo exit from early endosomes by the generation and elongation of recycling endosomal tubules in a process also involving adaptor protein 1 (AP-1), the kinesin-3 microtubule motor heavy-chain kinesin family member 13A (KIF13A), and phosphatidylinositol-4-phosphate kinases.[43–46]

Inactivating mutations in subunits of the obligate multi-subunit complex BLOC-1 are responsible for HPS-7, -8, -9, and -11, and corresponding mouse models *sandy*, *reduced pigmentation*, *pallid*, and *muted*, and result in the accumulation of key melanogenic cargoes, such as ATP7A, TYRP1, and OCA2, within early endosomes of melanocytes.[10,35,36,47] A cohort of these cargoes also leak into the degradative pathway.[34,35] A fraction of TYR is also dependent on BLOC-1 for its delivery to melanosomes and accumulates largely in late endosomes and lysosomes in BLOC-1-deficient melanocytes.[35,48] Nevertheless, a substantial subset of TYR is present within melanosomes of BLOC-1-deficient melanocytes but is minimally active—due at least in part to depletion of copper.[10] Although BLOC-1-deficient melanocytes from murine HPS models are severely hypopigmented, they are not completely devoid of melanin.[49,50] This suggests that despite the mislocalization of several key melanogenic proteins, BLOC-1-deficient melanocytes retain at least some basal melanogenic capacity. Here, we show that enhanced MC1R-cAMP signaling and/or direct neutralization of organelle pH of BLOC-1-deficient melanocytes increases melanin content but not within melanosomes. Instead, the melanin accumulates within late-endocytic organelles. The role of pH in regulating TYR activity and the dependence of pH regulators on BLOC-1 for targeting to melanosomes may partially explain the hypopigmentation phenotype observed in forms of BLOC-1-deficient HPS and the ability of MC1R signaling to partially restore pigmentation in a remodeled late endosome.

RESULTS

Prolonged MC1R/cAMP signaling enhances melanin content of BLOC-1-deficient melanocytes

Previous studies have used cAMP-elevating agents to stimulate the MC1R signaling pathway and increase photoprotective eumelanin within the skin.[20–22] We asked whether modulation of this pathway can enhance melanogenesis in cells that mistraffic melanogenic cargoes such as BLOC-1-deficient melanocytes. To test this, we compared the melanin content of wild-type (melan-a), BLOC-1-deficient (melan-pa, derived from *pallid* mice lacking the BLOC1S6 subunit of BLOC-1), and TYR-deficient (melan-c2, derived from albino mice) immortalized melanocytes that had been either unstimulated or cultured for 7 days with the cAMP-elevating agents cholera toxin (CT), NDP-MSH (a synthetic analog of α-MSH), or the adenylate cyclase activator forskolin. The unpigmented melan-c2 cell line expectedly did not respond to cAMP-elevating agents (Figure S1) and served as a negative control for the melanin assay.

Unstimulated wild-type melanocytes were pigmented, and melanin content increased upon treatment with cAMP-elevating agents, as shown by bright-field microscopy (Figure 1A) and validated by a quantitative melanin content assay (Figure 1C). These data are consistent with previous studies on the effects of enhanced MC1R signaling on melanocytes with competent trafficking machineries.[21,22,51]

In comparison, although unstimulated BLOC-1-deficient melanocytes were severely hypopigmented compared with wild-type melanocytes at steady-state as previously described,[35] treatment with cAMP-elevating agents increased pigmentation, as visualized by bright-field microscopy (Figure 1B) and confirmed by quantitative melanin content assay (Figure 1D). Similar results were obtained using another BLOC-1-deficient melanocyte line, melan-mu (derived from *muted* mice lacking the BLOC1S5 subunit; Figure S1), and the corresponding "rescued" line melan-mu:MuHA (BLOC-1^{R}; Figure S1). These data show that although melanin content of BLOC-1-deficient melanocytes is still much lower (by approximately 20-fold) than that of wild-type melanocytes, melanogenesis in BLOC-1-deficient melanocytes can be stimulated by cAMP-elevating agents despite the lack of a critical transport route to melanosomes.

Treatment with cAMP-elevating agents enhances melanogenic protein expression in BLOC-1-deficient melanocytes

We next tested whether increased melanogenic protein expression might contribute to the enhanced melanogenesis by cAMP-elevating agents in BLOC-1-deficient melanocytes. Expression of the crucial melanogenic enzyme TYR in wild-type (melan-a),

Please cite this article in press as: Goff et al., Reprogramming of endolysosomes for melanogenesis in BLOC-1-deficient melanocytes, Current Biology (2025), https://doi.org/10.1016/j.cub.2025.06.031

CellPress
OPEN ACCESS

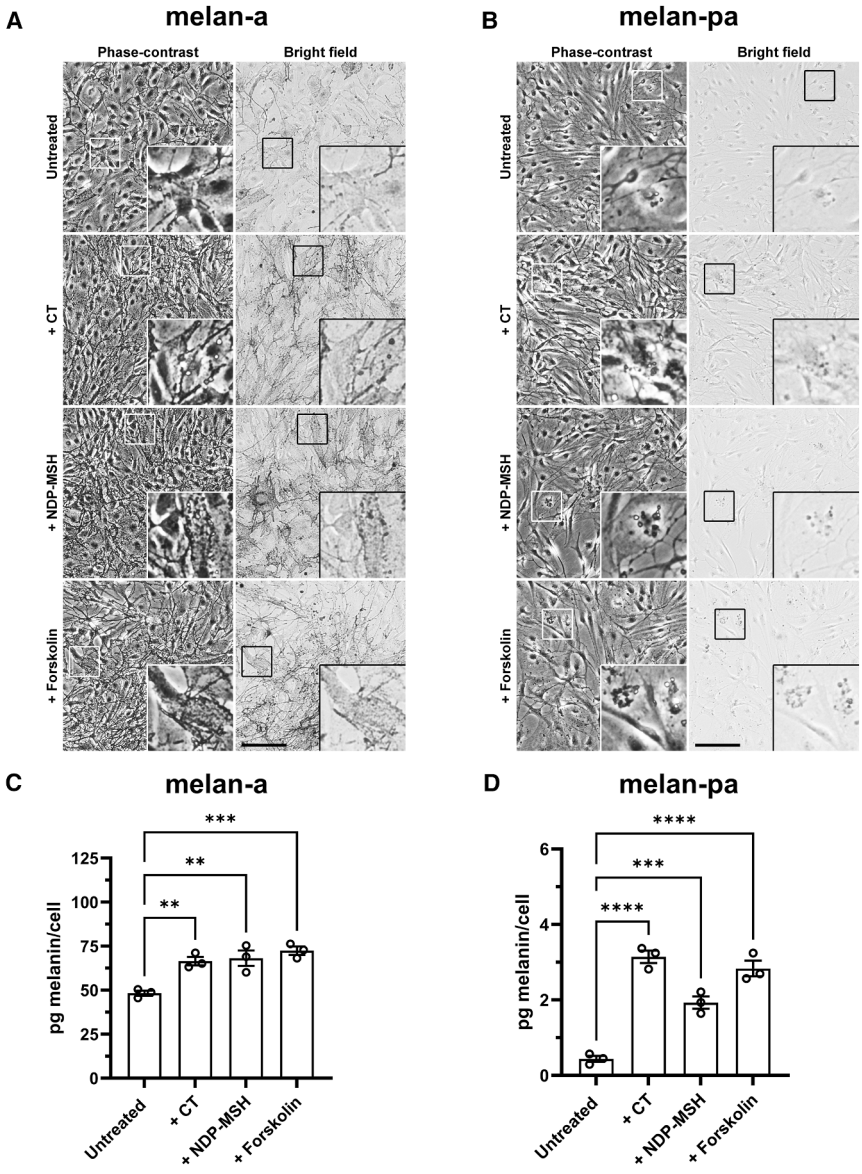

Figure 1. cAMP-elevating agents increase melanin content of wild-type and BLOC-1-deficient melanocytes

(A and B) Phase-contrast (left) and bright-field (right) microscopy of wild-type melanocytes (melan-a, A) or BLOC-1-deficient melanocytes (melan-pa, B), either untreated or treated with 200 nM CT, 100 pM NDP-MSH, or 20 μM forskolin for 7 days. Insets: boxed regions enlarged 3×. Scale bar, 100 μm.

(C and D) Quantification of melanin content of wild-type melan-a (C) or BLOC-1-deficient melan-pa (D) melanocytes cultured for 7 days in the presence or absence of either CT, NDP-MSH, or forskolin as described above. Data presented show the means of 3 independent experiments and are expressed as mean pg melanin/cell ± SEM. Statistical significance relative to the untreated control was determined by one-way ANOVA with Dunnett's multiple comparison test. $^{**}p < 0.01$; $^{***}p < 0.001$; $^{****}p < 0.0001$.

See also Figure S1.

BLOC-1-deficient (melan-pa and melan-mu), and "rescued" BLOC-1^{R} (melan-mu:MuHA, expressing HA-tagged human BLOC1S5) melanocytes treated for 7 days with cAMP-elevating agents was quantified via western blotting (Figure 2A). Interestingly, significant increases in TYR protein expression were only observed in BLOC-1-deficient melanocytes treated with cAMP-elevating agents and not in wild-type or BLOC-1^{R} melanocytes. The expression of other known melanogenic proteins (TYRP1 and PMEL) also showed a modest increase upon cAMP-elevating-agent treatment of BLOC-1-deficient melanocytes (Figures S2B and S2D) but not wild-type and BLOC-1^{R} melanocytes (Figures S2A and S2C). The data suggest that cAMP-elevating-agent-induced increases in melanin content of BLOC-1-deficient melanocytes may be, at least in part, due to enhanced expression of TYR and perhaps other melanogenic proteins. The steady-state levels of the melanogenic protein TYRP1 are reduced in BLOC-1-deficient melanocytes,[34] likely because of partial mislocalization to degradative organelles. Although TYR primarily follows a BLOC-1-independent/AP-3-dependent pathway to melanosomes,[48,52] TYR localization to melanosomes is also reduced in BLOC-1-deficient melanocytes.[35] Accordingly, quantitative western blotting showed that steady-state levels of TYR in BLOC-1-deficient (melan-mu and melan-pa) cells was reduced by ∼87% compared with wild-type melan-a melanocytes (Figure 2B). This may result from mislocalization and degradation of TYR as has been previously reported for TYRP1.[34,35]

To assess whether the increased TYR expression observed upon treatment with cAMP-elevating agents reflected increased synthesis and reduced degradation, or both, we measured TYR mRNA expression levels and protein stability before and after treatment. TYR mRNA expression, quantified by RT-qPCR (Figure S3A), showed significant increases in response to most cAMP-elevating agents in both BLOC-1-sufficient and -deficient cell lines. This suggests that some of the effect on TYR levels reflects increased synthesis. To test for degradation, we first incubated control and forskolin-treated BLOC-1-deficient melan-pa melanocytes for 8 h with Bafilomycin A1 (BafA1), an inhibitor of the vacuolar ATPase that acidifies post-Golgi compartments and that is required for lysosomal degradation. The data show a dramatic increase in TYR expression in both control and forskolin-treated cells (Figures S3B and S3C), suggesting that TYR is degraded by lysosomal proteolysis in both cases. However, the increase in expression was higher in untreated cells (4.1-fold) than in forskolin-treated cells (2.2-fold), suggesting that forskolin treatment might partially stabilize TYR by preventing lysosomal degradation. To further test this, we assessed the stability of TYR protein in BLOC-1-deficient melan-

Please cite this article in press as: Goff et al., Reprogramming of endolysosomes for melanogenesis in BLOC-1-deficient melanocytes, Current Biology (2025), https://doi.org/10.1016/j.cub.2025.06.031

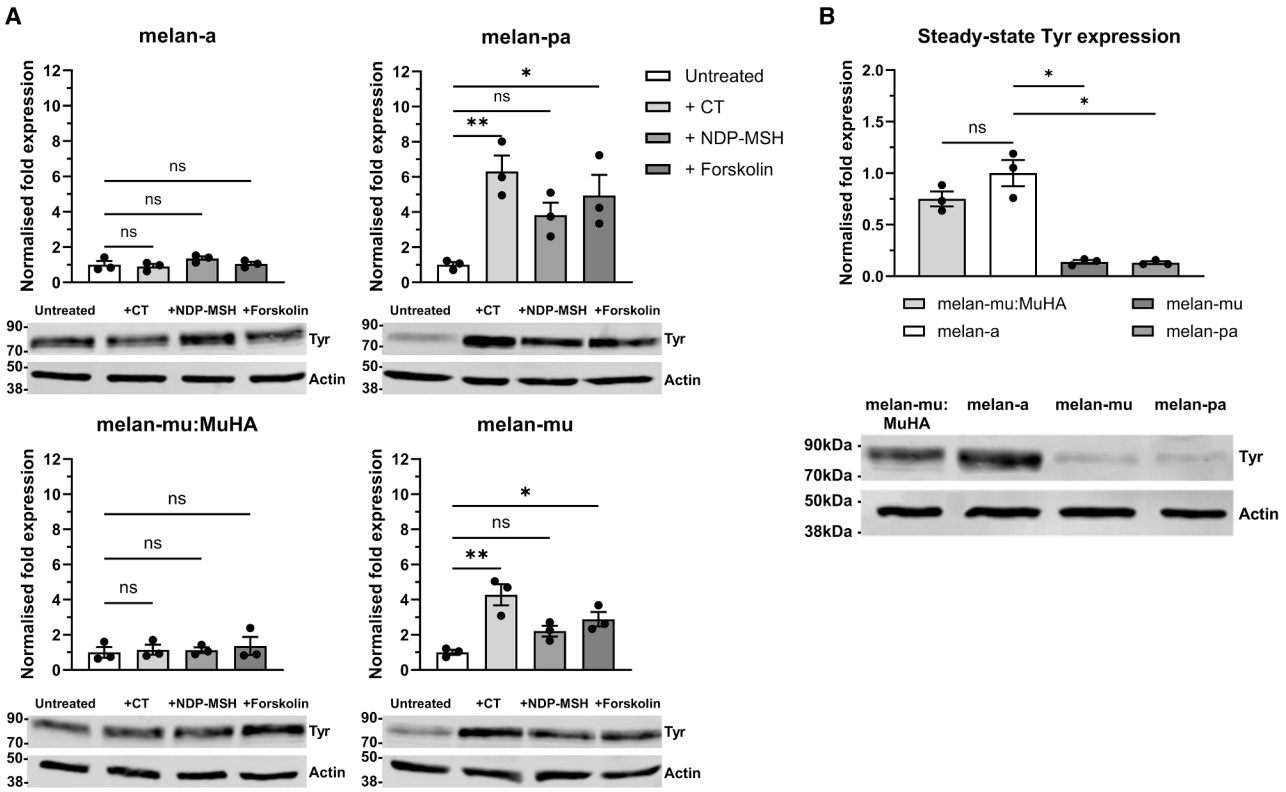

Figure 2. TYR protein expression in BLOC-1-deficient melanocytes is enhanced upon treatment with cAMP-elevating agents

BLOC-1-competent (wild-type melan-a and BLOC-1^{R} melan-mu:MuHA) and BLOC-1-deficient (melan-pa and melan-mu) melanocytes were cultured in the absence or presence of the indicated cAMP-elevating agents for 7 days, and then cell lysates were analyzed by western blotting for TYR and actin as a loading control. Representative blots are shown at the bottom, with positions of MW standards (in kDa) shown at the left, and quantifications from 3 independent biological replicates are shown at top. Quantitative data are the mean normalized fold expression of TYR protein relative to untreated control (A) or melan-a (B) ± SEM. Statistical significance relative to untreated control (A) or melan-a (B) TYR expression was determined by one-way ANOVA with Dunnett's multiple comparison test. ns, not significant; *$p < 0.05$; **$p < 0.01$.

See also Figures S2 and S3.

pa melanocytes by measuring the reduction of TYR protein expression upon treatment with the protein synthesis inhibitor, cycloheximide (CHX), over time via immunoblotting (Figures S3D and S3E). The data show that upon CHX treatment, TYR protein levels decay over time in both the absence and presence of forskolin, but that forskolin treatment doubles the half-life (7.08 h for untreated cells and 14.82 h for forskolin-treated cells). Treatment with BafA1 slowed the degradation in untreated cells and completely eliminated degradation in forskolin-treated cells (Figures S3F and S3G), indicating that all of the degradation in the latter reflected endolysosomal degradation. Taken together, these data show that forskolin both enhances TYR synthesis and reduces TYR degradation in BLOC-1-deficient melanocytes.

Melanin in BLOC-1-deficient melanocytes is predominantly formed within late-endosomal organelles

Cargoes destined for melanosomes primarily accumulate within early endosomes of BLOC-1-deficient melanocytes,[10,35,36] but a fraction of these proteins enter the degradative pathway[34]; for example, TYR localization to MVBs is increased nearly 4-fold in BLOC-1-deficient melanocytes compared with BLOC-1^{R} melanocytes,[35] consistent with the 4-fold increase in TYR levels upon BafA1 treatment in melan-pa cells (Figure S3). We therefore sought to assess in which compartments melanin accumulated in BLOC-1-deficient melanocytes.

Wild-type and BLOC-1-deficient melanocytes were cultured with or without forskolin, and melanin (visualized by bright-field microscopy) was localized relative to the mature melanosomal protein TYRP1 or the late endosomal/lysosomal membrane protein lysosome-associated membrane protein 2 (LAMP2) (visualized by immunofluorescence microscopy [IFM]). Melanin within wild-type melan-a (Figure 3A) and BLOC-1^{R} (data not shown, but see Setty et al.[35]) melanocytes overlapped with TYRP1-positive organelles and barely at all with LAMP2-positive organelles in both untreated and forskolin-treated cells (Figure 3A; quantified in Figure 3C). Similar results were observed in melan-a cultured with other cAMP-elevating agents (Figure S4A; quantified in Figure S4B). This indicates that, regardless of treatment, melanin within wild-type melanocytes accumulates as expected within melanosomes.

In contrast, melanin within BLOC-1-deficient melan-pa melanocytes overlapped only minimally with TYRP1-positive

Please cite this article in press as: Goff et al., Reprogramming of endolysosomes for melanogenesis in BLOC-1-deficient melanocytes, Current Biology (2025), https://doi.org/10.1016/j.cub.2025.06.031

CellPress
OPEN ACCESS

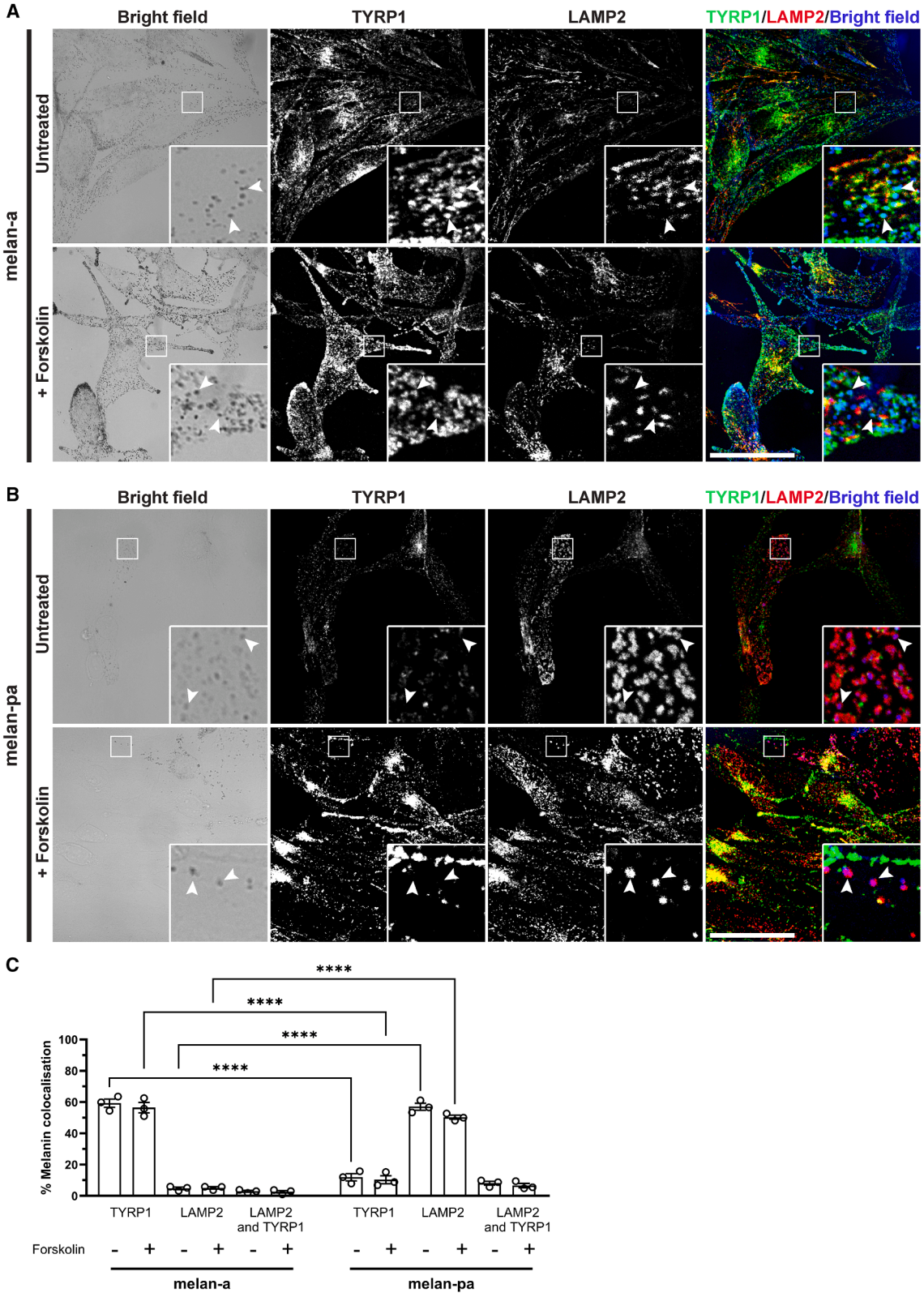

(legend on next page)

Please cite this article in press as: Goff et al., Reprogramming of endolysosomes for melanogenesis in BLOC-1-deficient melanocytes, Current Biology (2025), https://doi.org/10.1016/j.cub.2025.06.031

compartments (Figures 3B, 3C, and S4A), which correspond primarily to early endosomes[35] and, to a lesser extent, late endosomes, where it is likely degraded.[34] Melanin appeared to overlap with a small subset of LAMP2-positive structures irrespective of whether the cells were treated with cAMP-elevating agents (Figures 3B, 3C, and S4A). Despite the known targeting of TYRP1 to late endosomes and lysosomes in BLOC-1-deficient melanocytes, the percentage of total melanin that was found in compartments positive for both TYRP1 and LAMP2 was low and did not significantly differ from wild-type melanocytes. Similar results were seen in melan-mu, another BLOC-1-deficient melanocyte line (data not shown). The data suggest that melanin within BLOC-1-deficient melanocytes is formed not within bona fide melanosomes but rather in late endosomes or lysosomes that harbor LAMP2 and not intact TYRP1.

LAMP2 and the related protein LAMP1 are highly abundant on lysosomal membranes[53,54] but are also detected on late endosomes/multivesicular bodies (MVBs) and earlier endosomal compartments.[55–57] To better define where melanogenesis occurs in BLOC-1-deficient melanocytes and the nature of the LAMP2-containing organelles, we utilized both conventional transmission electron microscopy (TEM) and correlative light and electron microscopy (CLEM) analyses of the BLOC-1-deficient cell line melan-mu and BLOC-1^R melan-mu:MuHA, with or without forskolin treatment.

By TEM, BLOC-1^R melanocytes contained numerous melanosomes of all stages (stages I–IV) under control conditions (Figure 4A) and upon forskolin treatment (Figure 4B). The morphology of stage III and IV melanosomes in BLOC-1^R melanocytes was typical of these organelles, i.e., predominantly ellipsoid in shape, with striations visible within partially pigmented stage III organelles (Figures 4A′ and 4B′) and fully occluded within stage IV melanosomes (Figures 4A″ and 4B″). The mean length of the pigmented melanosomes in both untreated (428 ± 14 nm) and forskolin-treated (477 ± 17 nm) BLOC-1^R melanocytes (Figure 4G) is consistent with previous estimates of melanosomal length of approximately 500 nm.[58] In addition, the mean ratio of length to width is 1.77 ± 0.06 (untreated) and 1.97 ± 0.06 (forskolin treated), consistent with the observed ellipsoid shape of these organelles.

In contrast to the BLOC-1^R cells, TEM analysis of BLOC-1-deficient melanocytes showed many fewer pigmented structures, consistent with the melanin quantification in Figures 1D and S1C. As inferred from the IFM data, the few melanin deposits observed in either untreated (Figure 4C) or forskolin-treated (Figure 4D) BLOC-1-deficient melanocytes were not detected in bona fide ellipsoid and striated structures, which were abundant in these cells but not pigmented as previously described.[10,35] Rather, the pigment-containing organelles (Figures 4C–4F and accompanying insets) contained discrete clusters of melanin that appeared to surround and engulf intraluminal vesicles (ILVs) within MVBs. These organelles lacked the typical PMEL fibrils that are characteristic of stage II–IV melanosomes, were smaller in length than bona fide melanosomes (301 ± 8 nm for untreated and 280 ± 7 nm for forskolin treated), and had a more circular morphology (length to width ratio of 1.41 ± 0.04 untreated and 1.29 ± 0.03 for forskolin treated; Figure 4G). Thus, melanin is formed in BLOC-1-deficient cells in organelles with morphological characteristics of late endosomes and not in traditional melanosomes. Examples of unpigmented lysosomes in BLOC-1-deficient cells are shown in Figure S4C.

We further analyzed untreated and forskolin-treated BLOC-1-deficient melanocytes by CLEM. LAMP2-containing compartments with melanin pigments were identified by IFM and bright-field microscopy in fixed cells on dishes with a raised alphanumeric coverslip on the bottom, and then cells were processed for conventional TEM. Corresponding regions were identified and aligned with the IFM images. CLEM confirmed that the melanin-containing organelles in BLOC-1-deficient melanocytes were positive for LAMP2 and were ultra-structurally similar to MVBs rather than ellipsoid and striated melanosomes (Figures 4E and 4F). CLEM also confirmed that many LAMP2-containing structures lacked pigment. Taken together, these data show that melanin within BLOC-1-deficient melanocytes is formed within a subset of late endocytic compartments that closely resemble MVBs, likely by TYR and other melanosomal components in these compartments that are mislocalized due to the loss of BLOC-1.

A subpopulation of late endosomes/lysosomes of BLOC-1-deficient melanocytes has elevated pH

TYR is the rate-limiting enzyme and is absolutely necessary for melanogenesis to occur. Optimal TYR activity requires a near neutral environment[13,14,59]; TYR activity is abolished at pH < 5.5, levels that are typically reported for late endosomes and lysosomes. The detection of melanin in late endosomes (based on morphology) of BLOC-1-deficient melanocytes suggests that a subset of these typically acidic organelles must be at least partially neutralized and that this subset should be expanded upon treatment with cAMP-elevating agents—consistent with the increased TYR expression and half-life (Figure S3).

To test this, we determined the pH of late endosomes/lysosomes in melanocytes by exploiting uptake of a fluid-phase cargo, dextran, conjugated to Oregon green, a pH-dependent fluorophore. Cells were allowed to internalize Oregon green-dextran

Figure 3. Melanin in BLOC-1-deficient melanocytes resides in LAMP2-positive organelles

(A and B) Wild-type melan-a (A) or BLOC-1-deficient melan-pa (B) were treated or not with 20 μM forskolin for 7 days and then fixed, immunolabeled, and analyzed by confocal IFM and bright-field microscopy to determine the localization of melanin (visible in bright-field images) in relation to melanosomes (TYRP1, green) and late endosomes/lysosomes (LAMP2, red).

The bright-field images were inverted and pseudo-colored blue in the merged image at the right. Insets: boxed regions enlarged 4.5×. Arrowheads show overlap of melanin with TYRP1 but not LAMP2 in melan-a (A) or with LAMP2 but not TYRP1 in melan-pa (B). Scale bar, 50 μm.

(C) The percentage of total melanin that colocalized with either TYRP1, LAMP2, or both markers in untreated or forskolin-treated melan-a and melan-pa. Data represent mean ± SEM from 3 independent experiments (minimum 10 cells analyzed per experiment) with the following total number of cells: untreated melan-a 32, forskolin-treated melan-a 31, untreated melan-pa 30, and forskolin-treated melan-pa 32. Statistical significance was determined by one-way ANOVA with post hoc Tukey test, with only significant equivalent comparisons between cell lines shown. ****$p < 0.0001$.

See also Figure S4.

Please cite this article in press as: Goff et al., Reprogramming of endolysosomes for melanogenesis in BLOC-1-deficient melanocytes, Current Biology (2025), https://doi.org/10.1016/j.cub.2025.06.031

CellPress
OPEN ACCESS

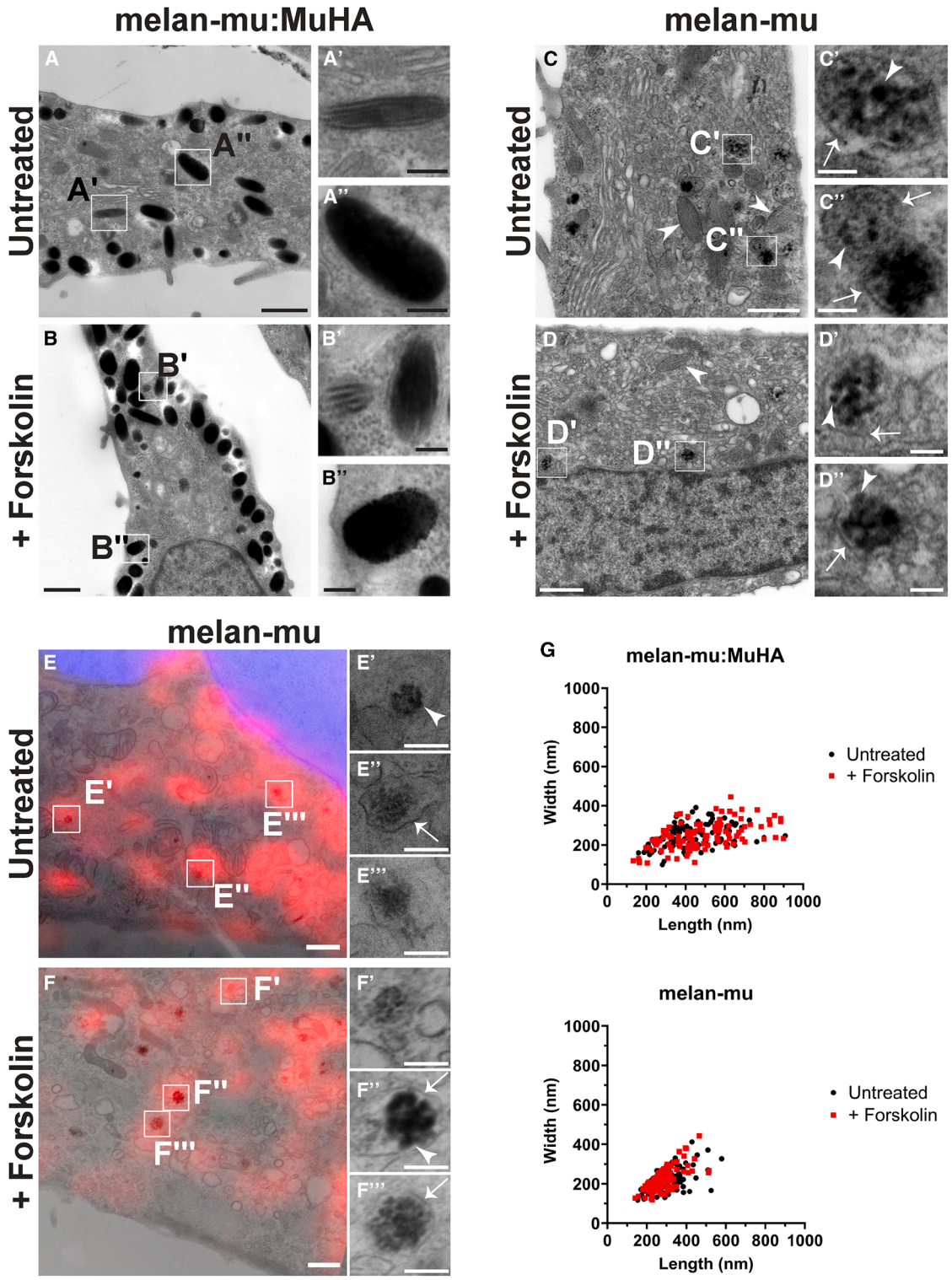

Figure 4. BLOC-1-deficient melanocytes produce melanin in LAMP2-positive organelles that resemble MVBs

(A–D) Conventional transmission electron microscopy analysis of untreated (A) or forskolin-treated (B) BLOC-1^{R} melanocytes (melan-mu:MuHA) or untreated (C) or forskolin-treated (D) BLOC-1-deficient melanocytes (melan-mu). Insets: 3× enlarged images of boxed regions in main panels. Arrowheads in (C) and (D) indicate unpigmented ellipsoid melanosomes. (A′) A partially pigmented stage III melanosome. (A″) A fully pigmented stage IV melanosome. (B′) A stage III and stage IV melanosome. (B″) A fully pigmented stage IV melanosome. (C′, C″, D′, and D″) Circular organelles containing vesicular melanin deposits.

(legend continued on next page)

Please cite this article in press as: Goff et al., Reprogramming of endolysosomes for melanogenesis in BLOC-1-deficient melanocytes, Current Biology (2025), https://doi.org/10.1016/j.cub.2025.06.031

(OG-D) for 16 h followed by a 2-h chase into late endosomes and lysosomes before analysis by fluorometry or imaging by wide-field fluorescent microscopy. The pH-dependent fluorescence of internalized OG-D was confirmed by fluorometry upon exposure to previously described calibration solutions,[60,61] both in a cell-free environment and in wild-type melanocytes (pKAs of 4.78 and 4.90, respectively; Figure S5A). The fluorometric assay was validated by the increased pH observed upon treating melanocytes with either BafA1 or methionine methyl ester (MME), a methylated amino acid that neutralizes esterase-containing organelles such as lysosomes,[62] with both agents known to neutralize lysosomal pH (Figure S5B). Using the labeling protocol above (also see STAR Methods), internalized OG-D in wild-type melanocytes overlapped extensively with expressed LAMP1-tdTomato when analyzed by wide-field fluorescent microscopy (Figure S5C), confirming that we were measuring the pH of late endosomes/lysosomes.

To measure lysosomal pH at steady state and in response to treatment with cAMP-elevating agents, wild-type, BLOC-1^{R}, and BLOC-1-deficient cell lines were cultured in the presence or absence of cAMP-elevating agents before labeling with OG-D as described above. Fluorometry was used to measure both the resting fluorescence and the maximal fluorescence observed upon cell exposure to ammonium chloride. Lysosomal pH was calculated using a previously described equation (Erent et al.[60]; STAR Methods) using the parameters obtained from *in vivo* calibration curves (Figure S5A). The data showed that in all melanocyte lines tested, the steady state pH of lysosomes is acidic (between pH 4.5 and 4.7), and treatment with cAMP-elevating agents did not significantly neutralize pH at the population level (Figure 5A). However, because previous reports have shown that lysosomal pH is heterogeneous,[63,64] we investigated the subcellular heterogeneity of late endosomes/lysosomes using high-magnification wide-field fluorescence microscopy in BLOC-1-deficient melanocytes that had internalized OG-D, as described above, and quantified the pH of individual late endosomes/lysosomes.

As expected, most OG-D-containing late endosomes/lysosomes were acidic (arrowheads, Figures 5B and 5C for quantification). However, a subset of organelles appeared to be more neutral with a pH closer to 6 (arrows, Figures 5B and 5C). Interestingly, the data showed that the mean intraluminal pH of late endosomes/lysosomes under control conditions is 4.7, and this increased to 5.1 upon treatment with the cAMP-elevating agent forskolin. This increase in mean luminal pH upon forskolin treatment was not observed at the population level (Figure 5A) and may reflect a bias toward measuring well-isolated peripheral OG-D-containing late endosomes/lysosomes rather than those within the perinuclear region, where individual structures could not be resolved. Taken together, the data show that the luminal pH of a subset of late endosomes/lysosomes in BLOC-1-deficient melanocytes is more neutral and can be further neutralized with forskolin treatment. These structures are therefore likely to facilitate TYR activity and subsequent melanogenesis. Unfortunately, we could not detect internalized OG-D within melanin-containing compartments to assess their pH. Potential reasons for this will be addressed in the discussion.

Genetic modulation of organelle pH is sufficient to enhance melanin outside of melanosomes

For melanogenesis to occur within the late endosomes of BLOC-1-deficient melanocytes, not only TYR but also other melanogenic proteins, including regulators of pH such as the chloride ion channel OCA2[11] and the putative proton/sugar transporter SLC45A2,[65] must be present to enable TYR activity. Within wild-type melanocytes, both OCA2 and SLC45A2 facilitate melanosome neutralization to promote melanogenesis,[11,12] both are classical targets of MITF, and at least OCA2 is targeted to melanosomes in a BLOC-1-dependent manner.[34–36] We hypothesize that despite the partial mislocalization of OCA2 and TYR to late endosomes upon loss of BLOC-1,[34,35] at steady state, BLOC-1-deficient melanocytes synthesize very little melanin within late endosomes, perhaps because OCA2 levels in these compartments are insufficient to modify the low pH that inhibits the activity of mislocalized TYR. Overexpression of OCA2 overcomes the loss of other transporters such as SLC45A2, resulting in partial restoration of pigmentation,[12] and when expressed in cells without LROs, OCA2 neutralizes late endosomes/lysosomes.[11,12] We therefore asked whether the overexpression of these regulators of organelle pH in BLOC-1-deficient melanocytes would partially neutralize the luminal pH of late endosomes, permitting the activation of mislocalized TYR and enhancing melanogenesis in these organelles.

To test this, we overexpressed HA-epitope-tagged forms of OCA2[66] or SLC45A2[12] in BLOC-1-deficient melan-mu melanocytes and assayed for pigmentation by bright-field microscopy (based on a previously described method[12]; see Figure S6A for examples of pigmentation scoring) and for lysosomal localization by IFM relative to LAMP2. The *Oca2*-null cell line, melan-p5, and the *Slc45a2*-null cell line, melan-uw, were included as positive controls. The data (Figure 6A; pigmentation quantified in Figure 6B) show that the overexpression of HA-OCA2, but not of HA-SLC45A2, enhances melanin content in BLOC-1-deficient melanocytes. Moreover, labeling for the HA-OCA2 transgene (via anti-HA tag labeling) colocalized with both melanin and LAMP2 (Figure 6A, quantified in 6C). A similar increase in pigmentation in LAMP2-positive structures was seen upon overexpression of HA-OCA2 in the BLOC-1-deficient line melan-pa (Figure S6C; pigmentation quantified in

(E–G) CLEM analysis of untreated (E) or forskolin-treated (F) BLOC-1-deficient melanocytes (melan-mu) immunolabeled for LAMP2 (red), with DAPI staining the nucleus (blue). Insets: 4× enlarged images of boxed regions in main panels. (E′–E‴) Ultrastructure of areas that are positive for LAMP2 in (E). (F′–F‴) Ultrastructure of areas that are positive for LAMP2 in (F). Arrowheads show melanin-encased ILVs within MVBs, the limiting membrane of which is shown by arrows. (G) Quantification of length and width of pigmented organelles in BLOC-1^{R} (melan-mu:MuHA) and BLOC-1-deficient (melan-mu) melanocytes cultured for 7 days with or without 20 μM forskolin. The length and width of a minimum of 100 pigmented organelles were obtained for each condition from electron microscopy images. No distinctions were made between different stages of melanosome maturation or whether the organelle was a bona fide melanosome. Scale bar in main panels, 800 nm. Scale bar insets, 200 nm.
See also Figure S4.

Please cite this article in press as: Goff et al., Reprogramming of endolysosomes for melanogenesis in BLOC-1-deficient melanocytes, Current Biology (2025), https://doi.org/10.1016/j.cub.2025.06.031

CellPress
OPEN ACCESS

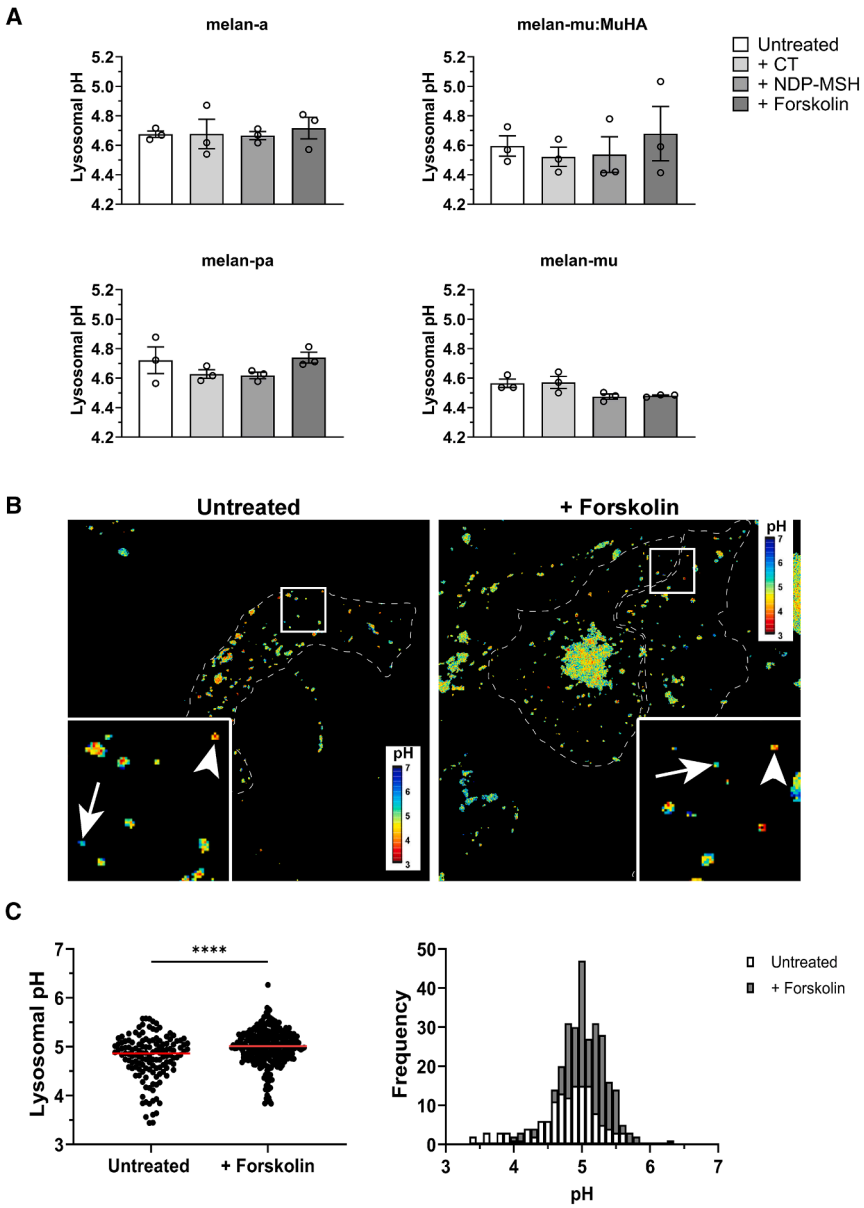

Figure 5. A subpopulation of late endosomes/lysosomes of BLOC-1-deficient melanocytes has elevated pH

BLOC-1-competent (melan-a and melan-mu:MuHA) and BLOC-1-deficient (melan-mu and melan-pa) melanocytes, cultured in the presence or absence of cAMP-elevating agents for 7 days, were exposed to Oregon green-dextran overnight and chased for 2 h to label late endosomes and lysosomes.

(A) Organellar pH was determined by fluorometry based on resting fluorescence relative to maximal fluorescence observed after exposure to ammonium chloride. Data represent mean ± SEM from 3 independent experiments. For each cell line, statistical analysis was performed by one-way ANOVA. No statistically significant differences were observed.

(B and C) Organellar fluorescence was assessed by live-cell imaging before and after exposure to ammonium chloride (B) and quantified in (C). Shown are pseudo-colored representations (note legend for scale) of the calculated lysosomal pH in untreated and forskolin-treated BLOC-1-deficient melanocytes. Arrows indicate lysosomes with a more neutral pH, and arrowheads indicate more acidic organelles. Insets: 3.5× enlarged image of boxed regions. Organellar pH was quantified from pseudo-colored representations. The pH of 309 (untreated) and 369 (forskolin-treated) individual organelles was quantified from 4 and 5 cells, respectively, across 3 independent experiments. Red line represents mean pH of organelles for each condition. Histogram represents binned values. Statistical analysis was determined by two-tailed Student's t test. ****$p < 0.0001$.

See also Figure S5.

Figure S6D; colocalization quantified in S6E). By contrast, overexpression of HA-OCA2 in hypopigmented *Oca2*-null melanocytes resulted in rescue of pigmentation (Figures 6A and 6B) but in structures that predominantly overlapped with HA-tag and not with labeling for LAMP2 (quantified Figure 6C), suggesting correct localization to melanosomes as previously documented.[12,66] Similar results were seen in *Slc45a2*-null melanocytes overexpressing HA-SLC45A2 (Figures 6A, 6B, and S6B). These data indicate that overexpression of OCA2 in BLOC-1-deficient melanocytes results in OCA2 delivery to a cohort of late endosomes/lysosomes, where it enhances melanin content. Because OCA2 and SLC45A2 are targets of microphthalmia-associated transcription factor (MITF), and hence upregulated by cAMP-dependent MC1R signalling,[67–69] this may in part explain why cAMP-elevating agents enhance pigmentation in BLOC-1-deficient melanocytes.

Direct neutralization of organelle pH rapidly increases melanin within late endosomes/lysosomes

Numerous studies have reported that deacidification agents can significantly enhance melanogenesis in TYR-positive amelanotic melanocytes.[13,70–74] The results of the approaches used thus far strongly suggest that neutralization of late endosomal compartments in BLOC-1-deficient melanocytes can elicit melanin synthesis by mistargeted TYR. To directly test the effects of neutralization of organelle pH on the melanin content of BLOC-1-deficient melanocytes, we assessed the effect on pigmentation of treatment with BafA1 and MME.

BLOC-1-deficient melan-mu cells were treated for 2 or 16 h with BafA1 or MME and visualized by bright-field microscopy (Figure 7A). Treatment with BafA1 led to a modest increase in visible pigmentation after 2 h and a much more dramatic increase after 16 h compared with the untreated control cells. Despite the relative specificity of MME in neutralizing lysosomes, the effects of treatment of MME on visible melanin were much more subtle and only detectable when visualized at higher magnification (Figure S7A). This may reflect either a more modest effect of MME on the pH of lysosomes compared with

Please cite this article in press as: Goff et al., Reprogramming of endolysosomes for melanogenesis in BLOC-1-deficient melanocytes, Current Biology (2025), https://doi.org/10.1016/j.cub.2025.06.031

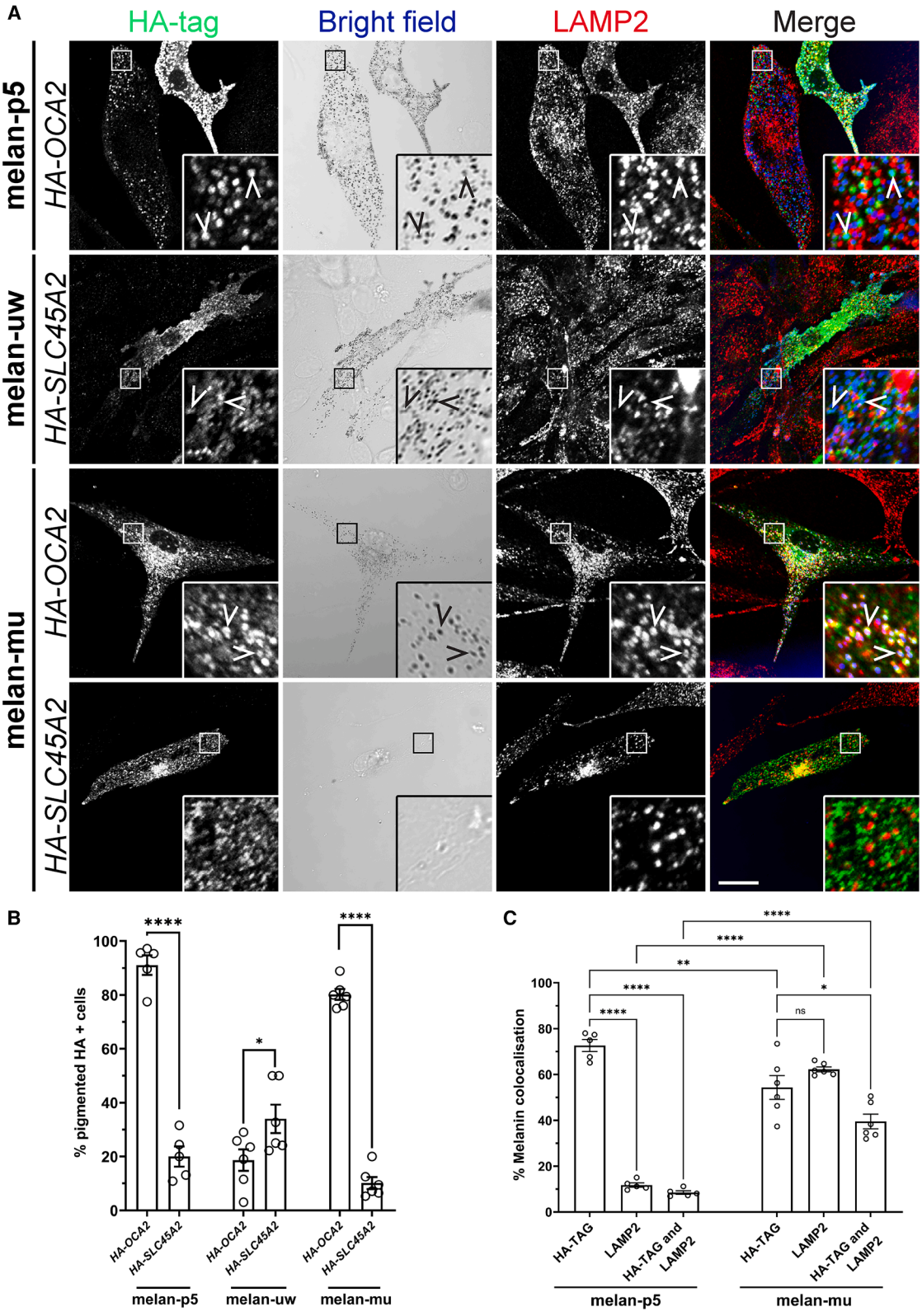

Figure 6. Overexpression of OCA2 in BLOC-1-deficient melanocytes partially restores pigmentation

Oca2-null melan-p5 cells, *Slc45a2*-null melan-uw cells, and BLOC-1-deficient melan-mu cells were transiently transfected with *HA-OCA2* or *HA-SLC45A2*, fixed and immunolabeled for HA and LAMP2, and analyzed by confocal IFM and bright-field microscopy to visualize melanin.

(legend continued on next page)

Please cite this article in press as: Goff et al., Reprogramming of endolysosomes for melanogenesis in BLOC-1-deficient melanocytes, Current Biology (2025), https://doi.org/10.1016/j.cub.2025.06.031

lysosomotropic compounds, as previously described[62] and shown in Figure S5B, or that the majority of melanogenesis occurs within esterase-negative late endosomes. Similar increases to that of BafA1 were observed using the less-specific deacidification agents, ammonium chloride, monensin, or nigericin (Figure S7B).

We next quantified the effects of BafA1 and MME on melanin content and asked whether the cAMP-elevating agent forskolin enhanced these effects. In wild-type (Figure 7B) and BLOC-1^R melanocytes (melan-mu:MuHA; Figure S7C), neither BafA1 nor MME treatment significantly enhanced basal or forskolin-stimulated melanin content. In contrast, co-treatment of BLOC-1-deficient melan-pa (Figure 7C) or melan-mu (Figure S7D) melanocytes with forskolin and either BafA1 or MME substantially increased melanin content relative to either treatment alone. Taken together these data suggest that direct pH neutralization rapidly activates pre-existing TYR and enhances melanin content specifically in BLOC-1-deficient melanocytes.

Lastly, we used IFM and bright-field microscopy to test for the localization of melanin within BLOC-1-deficient melanocytes treated with forskolin and either BafA1 or MME (Figures 7D and 7E). Although only cells treated with both forskolin and BafA1 harbored abundant well-pigmented melanin-containing granules, the melanin in all conditions resided within LAMP-2-containing structures, suggesting that they form in late endosomes/lysosomes and not in melanosomes.

DISCUSSION

Previous studies in BLOC-1-deficient melanocytes had described melanin in melanosomes with abnormal morphology; small, circular organelles without visible PMEL fibrils but often containing melanin-positive ILVs.[49,50,75,76] Here, we provide evidence to suggest that these organelles are in fact late endosomes or lysosomes. Analysis of the intra-organellar pH (pH_i) revealed a subpopulation of late endosomes/lysosomes with a pH_i that fell within the permissive range for TYR activity (>pH 5.5). Moreover, cargo upregulation due to enhanced MC1R signaling or raised pH_i due to genetic or pharmacological treatments led to enhanced melanin deposition in these organelles. Our data support the conclusion that mistargeting of melanosomal cargoes to late endosomes and lysosomes can reprogram these organelles to synthesize melanin under stimulated conditions.

The use of cAMP-elevating agents to increase melanin content has previously been established in cell lines and murine models with competent trafficking machineries.[21,22,51] Although our present study supports these observations in wild-type and BLOC-1^R melanocytes, we also show that BLOC-1-deficient melanocytes retain melanogenic capacity that can be enhanced with cAMP-elevating agents despite significant mislocalization of several melanogenic cargoes. The retention of melanogenic capabilities described here is consistent with both the coat color of BLOC-1-deficient mice and of skin samples from HPS-mutant mice,[49,50,77] which are not completely devoid of melanin. This contrasts with melanocytes derived from mice with pathogenic TYR mutations that result in the complete absence of melanin.[78] Although the cAMP-elevating-agent-induced increases in the melanin content of BLOC-1-deficient melanocytes are unlikely to be physiologically relevant, they do provide a potential therapeutic avenue for HPS patients and perhaps other trafficking disorders that warrants further research.

In this study, we show that melanin in BLOC-1-deficient melanocytes is predominantly formed not within melanosomes but rather within late endosomes or lysosomes. Melanogenesis within endolysosomes is not an entirely new concept, as TYR expressed exogenously within fibroblasts or HeLa cells localizes to late endosomes and lysosomes and generates melanin within these organelles.[79–81] However, in melanocytes, the melanosomes within which melanin is normally synthesized are distinct from endolysosomal compartments.[7] Nevertheless, previous studies have alluded to melanogenesis in endolysosomal organelles in BLOC-1-deficient melanocytes.[49,50,75,76] These studies show that, in BLOC-1-deficient melanocytes, melanin resides in small, circular organelles without visible PMEL fibrils but that often contain ILVs with melanin deposited on their outer membrane. Although these studies generally refer to these organelles as melanosomes, the current study strongly supports the idea that melanogenesis occurs in late endosomes in BLOC-1-deficient melanocytes as melanin resides in LAMP2-positive compartments that, by conventional electron microscopy and CLEM, resemble late endosomal MVBs in morphology; these organelles are smaller and more circular than traditional ellipsoid bona fide melanosomes. In addition, we noted that ellipsoid striated stage II melanosomes were present in BLOC-1-deficient melanocytes but remain unpigmented, in agreement with previous studies.[35,43] Surprisingly, these compartments largely remained unpigmented even upon treatment with deacidification agents, consistent with a previous study suggesting that these compartments lack the requisite copper cofactor for TYR due to the loss of ATP7A delivery to melanosomes.[10] It is intriguing that the ultrastructure of the MVB-like melanin-containing compartments resembles that of the compartments in which pheomelanin accumulates in melanocytes from red-haired individuals or MC1R mutant animals.[82–85]

(A) Shown are each individual channel and an overlay on the right in which pigment granules are pseudo-colored blue. Arrowheads indicate overlap between HA tag and melanin in *Oca2*-null cells expressing *HA-OCA2,* in *Slc45a2*-null cells expressing *HA-SLC45A2*, and between HA tag, LAMP2, and melanin in BLOC-1-deficient cells overexpressing *HA-OCA2*. Insets: boxed regions enlarged 4.5×. Scale bar, 20 μm.

(B) Quantification of the percentage of HA-positive *Oca2*-null melan-p5 cells, *Slc45a2*-null melan-uw cells and BLOC-1-deficient melan-mu cells that were pigmented. Data represent mean ± SEM from 5 (melan-p5) or 6 (melan-uw and melan-mu) independent experiments. Sample sizes: melan-p5, 188 SLC45A2 HA-positive cells and 171 OCA2 HA-positive cells; melan-uw, 186 SLC45A2 HA-positive cells and 176 OCA2 HA-positive cells; and melan-mu, 182 SLC45A2 HA-positive cells and 194 OCA2 HA-positive cells. Statistical significance relative to the % pigmented SLC45A2 HA-positive cells was determined for each cell line by two-tailed Student's t test. ****$p < 0.0001$.

(C) Quantification of the percentage of total melanin in melan-p5 and melan-mu expressing *HA-OCA2* that colocalized with HA-tag, LAMP2, or both markers. Data represent mean ± SEM from 5 (melan-p5) or 6 (melan-mu) independent experiments, with 30 total cells each for melan-p5 and melan-mu. Statistical significance was determined by one-way ANOVA with post hoc Tukey test. ns, not significant; *$p < 0.05$; **$p < 0.01$; ****$p < 0.0001$.

See also Figure S6.

Please cite this article in press as: Goff et al., Reprogramming of endolysosomes for melanogenesis in BLOC-1-deficient melanocytes, Current Biology (2025), https://doi.org/10.1016/j.cub.2025.06.031

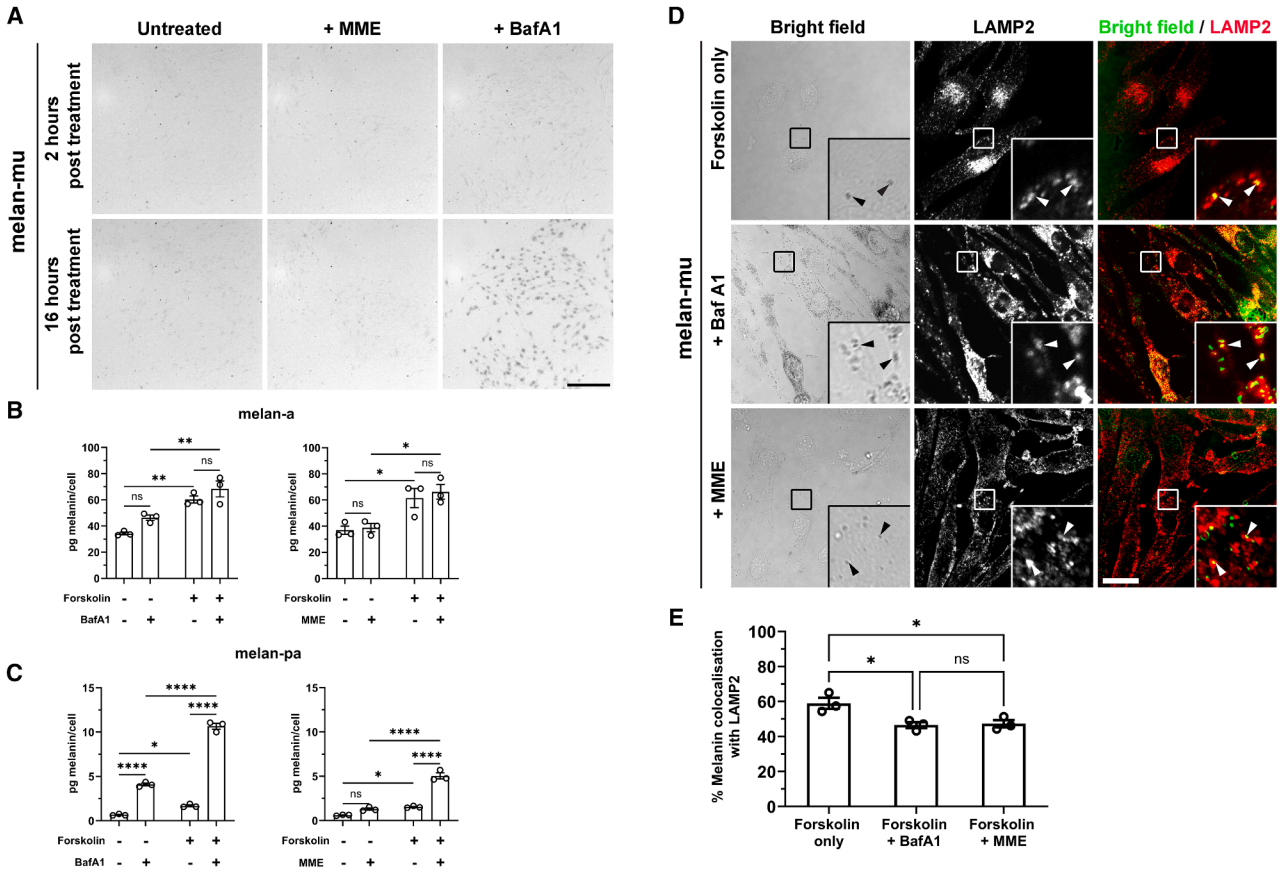

Figure 7. Direct pH neutralization by deacidification agents with or without forskolin significantly enhances melanin content in LAMP2-containing compartments of BLOC-1-deficient melanocytes

(A) Bright-field microscopy images of BLOC-1-deficient melan-mu melanocytes that were untreated or treated with 10 mM MME or 20 nM BafA1 analyzed at 2 and 16 h post treatment. Scale bar, 200 μm. (B and C) Quantitative melanin content analysis of wild-type melan-a melanocytes (B) or BLOC-1-deficient melan-pa melanocytes (C) cultured for 7 days in the absence or presence of 20 μM forskolin and either 20 nM BafA1 (for final 6 h) or 10 mM MME (for final 24 h). Data from 3 independent experiments are expressed as mean pg melanin/cell ± SEM. Statistical significance was determined by two-way ANOVA with a post hoc Tukey test. ns, not significant; $^{*}p < 0.05$; $^{**}p < 0.01$: $^{****}p < 0.0001$.

(D) BLOC-1-deficient melan-mu melanocytes treated with forskolin for 7 days and either BafA1 (for final 6 h) or MME for final 24 h were fixed, immunolabeled for LAMP2 (red), and analyzed by confocal IFM (for LAMP2) and bright-field microscopy (for pigment granules). Image shows each channel and a merged image in which the bright-field images were inverted and pseudo-colored green. Insets: boxed regions enlarged 4.5×. Arrowheads show puncta of LAMP2 overlapping with melanin. Scale bar, 20 μm.

(E) Quantification of the percentage of total melanin that colocalized with LAMP2 in melan-mu treated with forskolin for 7 days and either BafA1 (for final 6 h) or MME for final 24 h. Data represent mean ± SEM from 3 independent experiments (10 cells analyzed per experiment). Statistical significance was determined by one-way ANOVA with post hoc Tukey test. ns, not significant; $^{*}p < 0.05$.

See also Figure S7.

How does melanogenesis occur in late endosomes and how do cAMP-elevating agents increase the melanin content of BLOC-1-deficient melanocytes? Although cAMP-elevating agents had little effect on the protein content of TYR and other melanogenic proteins in BLOC-1-competent melanocytes at the time points analyzed here, these agents substantially increased melanogenic protein content in BLOC-1-deficient melanocytes, particularly for TYR, and reduced the rate of TYR degradation within late endosomes/lysosomes. Although TYR is crucial for melanogenesis, previous studies have shown that the activity and not the absolute expression level of TYR best correlates with melanin content.[14,86–88] This suggests that the cAMP-elevating-agent-induced increases in melanogenesis in both BLOC-1-competent and BLOC-1-deficient melanocytes may best reflect both increased TYR content and enhanced activity of the TYR present.

TYR activity requires near-neutral pH, and the expression of regulators of melanosome pH, such as OCA2 and SLC45A2, increase in response to cAMP-elevating agents.[51,69,89] It is therefore likely that the cAMP-induced increases in melanin of BLOC-1-deficient melanocytes are caused by a combination of increased TYR expression and increased expression of OCA2 and other proteins that facilitate enzymatic activity, all of which are likely mislocalized partially to late endosomes in the absence of BLOC-1. We speculate that only a subset of late endosomes accumulates sufficient levels of pH regulators and TYR to both deacidify the normally acidic late endosomes and facilitate TYR activity prior to degradation. This is supported by our data

Please cite this article in press as: Goff et al., Reprogramming of endolysosomes for melanogenesis in BLOC-1-deficient melanocytes, Current Biology (2025), https://doi.org/10.1016/j.cub.2025.06.031

showing that the luminal pH of a cohort of late endosomes/lysosomes is more neutral than the majority of such organelles. Indeed, other cell types harbor lysosomes with heterogeneous luminal pH.[63,64] We show that that the cohort of peripheral late endosomes/lysosomes with a more neutral pH can be increased upon treatment with forskolin, likely reflecting enhanced expression of proteins that regulate pH. The two methods to measure lysosomal pH in this study (fluorometric plate-based assay and live-cell microscopy) yielded slight differences in the mean values of lysosomal pH at steady state and in response to forskolin treatment. This is likely due to the differing conditions during measurement for both assays. The microscopy assay, unlike the fluorometric assay, does not take lysosomal volume of each compartment into consideration. The fluorometric assay is a global measure of the mean pH across hundreds of late endosomes/lysosomes and thousands of cells, whereas the values obtained from the microscopy assay represent the means from individual organelles and thus likely provide a more accurate representation of the heterogeneity of lysosomal pH. On the other hand, analyses with the microscopy assay are limited by the inability to resolve individual lysosomes in the densely populated perinuclear area and thus are skewed toward more peripheral lysosomes—which in other cells have been shown to be more neutral.[63,64] Despite these discrepancies, the values are quite close in both assays and we suggest that the more important point is that, when quantifying lysosomal pH via live-cell microscopy, lysosomal pH is heterogeneous (as others have already reported[63,64]) and a fraction of these lysosomes have a luminal pH permissive for TYR activity.

We show that purposeful overexpression of OCA2, a regulator of melanosomal pH, enhances melanogenesis in BLOC-1-deficient melanocytes, likely due to partial neutralization of late endosomes. We speculate that OCA2, a known BLOC-1-dependent cargo, is mislocalized to late endosomes like other BLOC-1-dependent cargoes,[34,35] alongside a cohort of TYR,[34,35] but that endogenous expression of OCA2 is relatively low and insufficient to neutralize luminal pH to facilitate substantial TYR activity. We further speculate that the increase in OCA2 expression upon treatment with cAMP-elevating agents leads to enhanced late endosome neutralization and hence more melanin synthesis, and the purposeful overexpression of OCA2 leads to a significant increase in melanin content in late endosomes. We suggest that this reflects both a substantial increase in the mislocalization of a cohort of OCA2 to late endosomes and the pH neutralizing effect of OCA2 chloride channel activity,[11] although direct measurement of organelle pH in response to OCA2 overexpression was not possible in this study. In contrast to this, the overexpression of SLC45A2 did not significantly enhance melanin content. This may reflect a putative role for SLC45A2 in maintaining the organelle pH gradient that is first established by OCA2[12] rather than in establishing such a gradient. In support of our hypothesis that partial neutralization of organelle pH is a key driver of enhanced melanogenesis of BLOC-1-deficient melanocytes, direct neutralization of organelle pH by treatment with BafA1 or MME rapidly and significantly increased melanin content in BLOC-1-deficient but not wild-type melanocytes. This suggests that melanosome pH is already optimal for melanogenesis within wild-type melanocytes, whereas most late endosomes in BLOC-1-deficient melanocytes are too acidic to support melanogenesis. Although the import of copper into melanosomes by the copper transporter ATP7A is necessary for TYR activity in wild-type melanocytes and is disrupted in BLOC-1-deficient melanocytes, excess copper was unable to restore TYR activity at an acidic pH,[10] indicating that pH may also play an important role in the hypopigmentation phenotype of BLOC-1-deficient melanocytes. The current study supports this interpretation, and the cohort of ATP7A that mislocalizes to multivesicular late endosomes in these cells[10] likely supplies sufficient copper cofactor to activate TYR within the deacidified organelles.

In summary, we propose that a cohort of inactive TYR is mislocalized to late endosomal MVBs in BLOC-1-deficient melanocytes. Within these organelles, TYR encounters mislocalized BLOC-1-dependent cargoes—including OCA2, ATP7A, and perhaps SLC45A2—that could facilitate melanogenesis within late-endocytic organelles. Increased expression of melanogenic proteins (via enhanced MC1R signaling) and/or increase of pH (either via enhanced MC1R signaling, genetic manipulation, or the use of deacidification agents) further increases melanin content by facilitating TYR activity in late endosomal MVBs. This work extends our understanding of the hypopigmentation phenotype of BLOC-1-deficient melanocytes and documents a novel mechanism of organelle reprogramming to allow for melanogenesis in the absence of functional melanosomes.

RESOURCE AVAILABILITY

Lead contact

Further information and requests for resources and reagents should be directed to, and will be fulfilled by, the lead contact, Michael Marks (marksm@pennmedicine.upenn.edu).

Materials availability

Cell lines used in this study are available from the Functional Genomics Cell Bank at City St. George's University of London, London, UK.

Data and code availability

- All data reported in this paper will be shared by the lead contact upon request.
- This paper does not report original code.
- Any additional information required to reanalyze the data reported in this paper is available from the lead contact upon request.

ACKNOWLEDGMENTS

The authors are grateful to Dr. Matthew Hannah and Dr. Heather Brooks for practical help and advice regarding electron microscopy studies and to Dr. Nyamekye Obeng-Adjei for preliminary studies that led to this work. We are grateful for funding from the Wellcome Trust (grant number 108429/Z/15/Z to E.V.S.) and US National Institutes of Health grant R01EY015625 to M.S.M. (from the National Eye Institute).

AUTHOR CONTRIBUTIONS

Conceptualization, P.S.G., E.V.S., and M.S.M.; methodology, P.S.G., T.C., M.S.M., and E.V.S.; investigation, P.S.G., D.C.H., and S.P.; resources, T.C. and M.S.M.; writing – original draft, P.S.G.; writing – review & editing, P.S.G., S.P., D.C.H., T.C., M.S.M., and E.V.S.; visualization, P.S.G.; supervision, T.C., E.V.S., and M.S.M.; funding acquisition, E.V.S. and M.S.M.

DECLARATION OF INTERESTS

The authors declare no competing interests.

STAR★METHODS

Detailed methods are provided in the online version of this paper and include the following:

- KEY RESOURCES TABLE
- EXPERIMENTAL MODEL AND STUDY PARTICIPANT DETAILS
- METHOD DETAILS
  - Intracellular melanin content
  - Western blotting and quantification
  - Cycloheximide chase assay
  - Quantitative Reverse Transcription Polymerase Chain Reaction (RT-qPCR)
  - Immunolabelling, Immunofluorescence Microscopy and colocalization analysis
  - Conventional transmission electron microscopy and quantification of pigmented organelles
  - Correlative light and electron microscopy (CLEM)
  - Transfection and quantification
  - Lysosomal pH measurements
- QUANTIFICATION AND STATISTICAL ANALYSIS

SUPPLEMENTAL INFORMATION

Supplemental information can be found online at https://doi.org/10.1016/j.cub.2025.06.031.

Received: July 8, 2024
Revised: April 10, 2025
Accepted: June 10, 2025

REFERENCES

1. Bowman, S.L., Bi-Karchin, J., Le, L., and Marks, M.S. (2019). The road to lysosome-related organelles: Insights from Hermansky-Pudlak syndrome and other rare diseases. Traffic *20*, 404–435. https://doi.org/10.1111/tra.12646.
2. Kobayashi, N., Nakagawa, A., Muramatsu, T., Yamashina, Y., Shirai, T., Hashimoto, M.W., Ishigaki, Y., Ohnishi, T., and Mori, T. (1998). Supranuclear melanin caps reduce ultraviolet induced DNA photoproducts in human epidermis. J. Invest. Dermatol. *110*, 806–810. https://doi.org/10.1046/j.1523-1747.1998.00178.x.
3. Graham, D.G., Tiffany, S.M., and Vogel, F.S. (1978). The toxicity of melanin precursors. J. Invest. Dermatol. *70*, 113–116. https://doi.org/10.1111/1523-1747.ep12541249.
4. Hochstein, P., and Cohen, G. (1963). The cytotoxicity of melanin precursors. Ann. N. Y. Acad. Sci. *100*, 876–886. https://doi.org/10.1111/j.1749-6632.1963.tb42896.x.
5. Benito-Martínez, S., Salavessa, L., Raposo, G., Marks, M.S., and Delevoye, C. (2021). Melanin transfer and fate within keratinocytes in human skin pigmentation. Integr. Comp. Biol. *61*, 1546–1555. https://doi.org/10.1093/icb/icab094.
6. Seiji, M., Fitzpatrick, T.B., Simpson, R.T., and Birbeck, M.S.C. (1963). Chemical composition and terminology of specialized organelles (melanosomes and melanin granules) in mammalian melanocytes. Nature *197*, 1082–1084. https://doi.org/10.1038/1971082a0.
7. Raposo, G., Tenza, D., Murphy, D.M., Berson, J.F., and Marks, M.S. (2001). Distinct protein sorting and localization to premelanosomes, melanosomes, and lysosomes in pigmented melanocytic cells. J. Cell Biol. *152*, 809–824. https://doi.org/10.1083/jcb.152.4.809.
8. Hurbain, I., Geerts, W.J.C., Boudier, T., Marco, S., Verkleij, A.J., Marks, M.S., and Raposo, G. (2008). Electron tomography of early melanosomes: implications for melanogenesis and the generation of fibrillar amyloid sheets. Proc. Natl. Acad. Sci. USA *105*, 19726–19731. https://doi.org/10.1073/pnas.0803488105.
9. Hellström, A.R., Watt, B., Fard, S.S., Tenza, D., Mannström, P., Narfström, K., Ekesten, B., Ito, S., Wakamatsu, K., Larsson, J., et al. (2011). Inactivation of Pmel alters melanosome shape but has only a subtle effect on visible pigmentation. PLOS Genet. *7*, e1002285. https://doi.org/10.1371/journal.pgen.1002285.
10. Setty, S.R.G., Tenza, D., Sviderskaya, E.V., Bennett, D.C., Raposo, G., and Marks, M.S. (2008). Cell-specific ATP7A transport sustains copper-dependent tyrosinase activity in melanosomes. Nature *454*, 1142–1146. https://doi.org/10.1038/nature07163.
11. Bellono, N.W., Escobar, I.E., Lefkovith, A.J., Marks, M.S., and Oancea, E. (2014). An intracellular anion channel critical for pigmentation. eLife *3*, e04543. https://doi.org/10.7554/eLife.04543.
12. Le, L., Escobar, I.E., Ho, T., Lefkovith, A.J., Latteri, E., Haltaufderhyde, K. D., Dennis, M.K., Plowright, L., Sviderskaya, E.V., Bennett, D.C., et al. (2020). SLC45A2 protein stability and regulation of melanosome pH determine melanocyte pigmentation. Mol. Biol. Cell *31*, 2687–2702. https://doi.org/10.1091/mbc.E20-03-0200.
13. Ancans, J., Tobin, D.J., Hoogduijn, M.J., Smit, N.P., Wakamatsu, K., and Thody, A.J. (2001). Melanosomal pH controls rate of melanogenesis, eumelanin/phaeomelanin ratio and melanosome maturation in melanocytes and melanoma cells. Exp. Cell Res. *268*, 26–35. https://doi.org/10.1006/excr.2001.5251.
14. Fuller, B.B., Spaulding, D.T., and Smith, D.R. (2001). Regulation of the catalytic activity of preexisting tyrosinase in black and Caucasian human melanocyte cell cultures. Exp. Cell Res. *262*, 197–208. https://doi.org/10.1006/excr.2000.5092.
15. Bertolotto, C., Abbe, P., Hemesath, T.J., Bille, K., Fisher, D.E., Ortonne, J.P., and Ballotti, R. (1998). Microphthalmia gene product as a signal transducer in cAMP-induced differentiation of melanocytes. J. Cell Biol. *142*, 827–835. https://doi.org/10.1083/jcb.142.3.827.
16. Price, E.R., Horstmann, M.A., Wells, A.G., Weilbaecher, K.N., Takemoto, C.M., Landis, M.W., and Fisher, D.E. (1998). alpha-Melanocyte-stimulating hormone signaling regulates expression of microphthalmia, a gene deficient in Waardenburg syndrome. J. Biol. Chem. *273*, 33042–33047. https://doi.org/10.1074/jbc.273.49.33042.
17. Bertolotto, C., Buscà, R., Abbe, P., Bille, K., Aberdam, E., Ortonne, J.P., and Ballotti, R. (1998). Different cis-acting elements are involved in the regulation of TRP1 and TRP2 promoter activities by cyclic AMP: pivotal role of M boxes (GTCATGTGCT) and of microphthalmia. Mol. Cell. Biol. *18*, 694–702. https://doi.org/10.1128/MCB.18.2.694.
18. Levine, N., Sheftel, S.N., Eytan, T., Dorr, R.T., Hadley, M.E., Weinrach, J. C., Ertl, G.A., Toth, K., McGee, D.L., and Hruby, V.J. (1991). Induction of skin tanning by subcutaneous administration of a potent synthetic melanotropin. JAMA *266*, 2730–2736. https://doi.org/10.1001/jama.1991.03470190078033.
19. Barnetson, R.S., Ooi, T.K.T., Zhuang, L., Halliday, G.M., Reid, C.M., Walker, P.C., Humphrey, S.M., and Kleinig, M.J. (2006). [Nle4-D-Phe7]-alpha-melanocyte-stimulating hormone significantly increased pigmentation and decreased UV damage in fair-skinned Caucasian volunteers. J. Invest. Dermatol. *126*, 1869–1878. https://doi.org/10.1038/sj.jid.5700317.
20. Bautista, R.M., Carter, K.M., Jarrett, S.G., Napier, D., Wakamatsu, K., Ito, S., and D'Orazio, J.A. (2020). Cutaneous pharmacologic cAMP induction induces melanization of the skin and improves recovery from ultraviolet injury in melanocortin 1 receptor-intact or heterozygous skin. Pigment Cell Melanoma Res. *33*, 30–40. https://doi.org/10.1111/pcmr.12817.
21. D'Orazio, J.A., Nobuhisa, T., Cui, R., Arya, M., Spry, M., Wakamatsu, K., Igras, V., Kunisada, T., Granter, S.R., Nishimura, E.K., et al. (2006). Topical drug rescue strategy and skin protection based on the role of Mc1r in UV-induced tanning. Nature *443*, 340–344. https://doi.org/10.1038/nature05098.
22. Spry, M.L., Vanover, J.C., Scott, T., Abona-Ama, O., Wakamatsu, K., Ito, S., and D'Orazio, J.A. (2009). Prolonged treatment of fair-skinned mice with topical forskolin causes persistent tanning and UV protection.

Pigment Cell Melanoma Res. *22*, 219–229. https://doi.org/10.1111/j.1755-148X.2008.00536.x.

23. Hermansky, F., and Pudlak, P. (1959). Albinism associated with hemorrhagic diathesis and unusual pigmented reticular cells in the bone marrow: report of two cases with histochemical studies. Blood *14*, 162–169. https://doi.org/10.1182/blood-2016-01-696435.
24. Ammann, S., Schulz, A., Krägeloh-Mann, I., Dieckmann, N.M.G., Niethammer, K., Fuchs, S., Eckl, K.M., Plank, R., Werner, R., Altmüller, J., et al. (2016). Mutations in AP3D1 associated with immunodeficiency and seizures define a new type of Hermansky-Pudlak syndrome. Blood *127*, 997–1006. https://doi.org/10.1182/blood-2015-09-671636.
25. Anikster, Y., Huizing, M., White, J., Shevchenko, Y.O., Fitzpatrick, D.L., Touchman, J.W., Compton, J.G., Bale, S.J., Swank, R.T., Gahl, W.A., et al. (2001). Mutation of a new gene causes a unique form of Hermansky-Pudlak syndrome in a genetic isolate of central Puerto Rico. Nat. Genet. *28*, 376–380. https://doi.org/10.1038/ng576.
26. Badolato, R., Prandini, A., Caracciolo, S., Colombo, F., Tabellini, G., Giacomelli, M., Cantarini, M.E., Pession, A., Bell, C.J., Dinwiddie, D.L., et al. (2012). Exome sequencing reveals a pallidin mutation in a Hermansky-Pudlak-like primary immunodeficiency syndrome. Blood *119*, 3185–3187. https://doi.org/10.1182/blood-2012-01-404350.
27. Dell'Angelica, E.C., Shotelersuk, V., Aguilar, R.C., Gahl, W.A., and Bonifacino, J.S. (1999). Altered trafficking of lysosomal proteins in Hermansky-Pudlak syndrome due to mutations in the beta 3A subunit of the AP-3 adaptor. Mol. Cell *3*, 11–21. https://doi.org/10.1016/s1097-2765(00)80170-7.
28. Li, W., Zhang, Q., Oiso, N., Novak, E.K., Gautam, R., O'Brien, E.P., Tinsley, C.L., Blake, D.J., Spritz, R.A., Copeland, N.G., et al. (2003). Hermansky-Pudlak syndrome type 7 (HPS-7) results from mutant dysbindin, a member of the biogenesis of lysosome-related organelles complex 1 (BLOC-1). Nat. Genet. *35*, 84–89. https://doi.org/10.1038/ng1229.
29. Morgan, N.V., Pasha, S., Johnson, C.A., Ainsworth, J.R., Eady, R.A.J., Dawood, B., McKeown, C., Trembath, R.C., Wilde, J., Watson, S.P., et al. (2006). A germline mutation in BLOC1S3/reduced pigmentation causes a novel variant of Hermansky-Pudlak syndrome (HPS8). Am. J. Hum. Genet. *78*, 160–166. https://doi.org/10.1086/499338.
30. Oh, J., Bailin, T., Fukai, K., Feng, G.H., Ho, L., Mao, J.I., Frenk, E., Tamura, N., and Spritz, R.A. (1996). Positional cloning of a gene for Hermansky-Pudlak syndrome, a disorder of cytoplasmic organelles. Nat. Genet. *14*, 300–306. https://doi.org/10.1038/ng1196-300.
31. Pennamen, P., Le, L., Tingaud-Sequeira, A., Fiore, M., Bauters, A., Van Duong Béatrice, N., Coste, V., Bordet, J.C., Plaisant, C., Diallo, M., et al. (2020). BLOC1S5 pathogenic variants cause a new type of Hermansky-Pudlak syndrome. Genet. Med. *22*, 1613–1622. https://doi.org/10.1038/s41436-020-0867-5.
32. Suzuki, T., Li, W., Zhang, Q., Karim, A., Novak, E.K., Sviderskaya, E.V., Hill, S.P., Bennett, D.C., Levin, A.V., Nieuwenhuis, H.K., et al. (2002). Hermansky-Pudlak syndrome is caused by mutations in HPS4, the human homolog of the mouse light-ear gene. Nat. Genet. *30*, 321–324. https://doi.org/10.1038/ng835.
33. Zhang, Q., Zhao, B., Li, W., Oiso, N., Novak, E.K., Rusiniak, M.E., Gautam, R., Chintala, S., O'Brien, E.P., Zhang, Y., et al. (2003). Ru2 and Ru encode mouse orthologs of the genes mutated in human Hermansky-Pudlak syndrome types 5 and 6. Nat. Genet. *33*, 145–153. https://doi.org/10.1038/ng1087.
34. Di Pietro, S.M., Falcón-Pérez, J.M., Tenza, D., Setty, S.R.G., Marks, M.S., Raposo, G., and Dell'Angelica, E.C. (2006). BLOC-1 interacts with BLOC-2 and the AP-3 complex to facilitate protein trafficking on endosomes. Mol. Biol. Cell *17*, 4027–4038. https://doi.org/10.1091/mbc.e06-05-0379.
35. Setty, S.R.G., Tenza, D., Truschel, S.T., Chou, E., Sviderskaya, E.V., Theos, A.C., Lamoreux, M.L., Di Pietro, S.M., Starcevic, M., Bennett, D.C., et al. (2007). BLOC-1 is required for cargo-specific sorting from vacuolar early endosomes toward lysosome-related organelles. Mol. Biol. Cell *18*, 768–780. https://doi.org/10.1091/mbc.e06-12-1066.
36. Sitaram, A., Dennis, M.K., Chaudhuri, R., De Jesus-Rojas, W., Tenza, D., Setty, S.R.G., Wood, C.S., Sviderskaya, E.V., Bennett, D.C., Raposo, G., et al. (2012). Differential recognition of a dileucine-based sorting signal by AP-1 and AP-3 reveals a requirement for both BLOC-1 and AP-3 in delivery of OCA2 to melanosomes. Mol. Biol. Cell *23*, 3178–3192. https://doi.org/10.1091/mbc.E11-06-0509.
37. Ciciotte, S.L., Gwynn, B., Moriyama, K., Huizing, M., Gahl, W.A., Bonifacino, J.S., and Peters, L.L. (2003). Cappuccino, a mouse model of Hermansky-Pudlak syndrome, encodes a novel protein that is part of the pallidin-muted complex (BLOC-1). Blood *101*, 4402–4407. https://doi.org/10.1182/blood-2003-01-0020.
38. Falcón-Pérez, J.M., Starcevic, M., Gautam, R., and Dell'Angelica, E.C. (2002). BLOC-1, a novel complex containing the pallidin and muted proteins involved in the biogenesis of melanosomes and platelet-dense granules. J. Biol. Chem. *277*, 28191–28199. https://doi.org/10.1074/jbc.M204011200.
39. Gwynn, B., Martina, J.A., Bonifacino, J.S., Sviderskaya, E.V., Lamoreux, M.L., Bennett, D.C., Moriyama, K., Huizing, M., Helip-Wooley, A., Gahl, W.A., et al. (2004). Reduced pigmentation (rp), a mouse model of Hermansky-Pudlak syndrome, encodes a novel component of the BLOC-1 complex. Blood *104*, 3181–3189. https://doi.org/10.1182/blood-2004-04-1538.
40. Moriyama, K., and Bonifacino, J.S. (2002). Pallidin is a component of a multi-protein complex involved in the biogenesis of lysosome-related organelles. Traffic *3*, 666–677. https://doi.org/10.1034/j.1600-0854.2002.30908.x.
41. Starcevic, M., and Dell'Angelica, E.C. (2004). Identification of snapin and three novel proteins (BLOS1, BLOS2, and BLOS3/reduced pigmentation) as subunits of biogenesis of lysosome-related organelles complex-1 (BLOC-1). J. Biol. Chem. *279*, 28393–28401. https://doi.org/10.1074/jbc.M402513200.
42. Lee, H.H., Nemecek, D., Schindler, C., Smith, W.J., Ghirlando, R., Steven, A.C., Bonifacino, J.S., and Hurley, J.H. (2012). Assembly and architecture of biogenesis of lysosome-related organelles complex-1 (BLOC-1). J. Biol. Chem. *287*, 5882–5890. https://doi.org/10.1074/jbc.M111.325746.
43. Delevoye, C., Heiligenstein, X., Ripoll, L., Gilles-Marsens, F., Dennis, M.K., Linares, R.A., Derman, L., Gokhale, A., Morel, E., Faundez, V., et al. (2016). BLOC-1 brings together the actin and microtubule cytoskeletons to generate recycling endosomes. Curr. Biol. *26*, 1–13. https://doi.org/10.1016/j.cub.2015.11.020.
44. Delevoye, C., Miserey-Lenkei, S., Montagnac, G., Gilles-Marsens, F., Paul-Gilloteaux, P., Giordano, F., Waharte, F., Marks, M.S., Goud, B., and Raposo, G. (2014). Recycling endosome tubule morphogenesis from sorting endosomes requires the kinesin motor KIF13A. Cell Rep. *6*, 445–454. https://doi.org/10.1016/j.celrep.2014.01.002.
45. Jani, R.A., Di Cicco, A., Keren-Kaplan, T., Vale-Costa, S., Hamaoui, D., Hurbain, I., Tsai, F.C., Di Marco, M., Macé, A.S., Zhu, Y., et al. (2022). PI4P and BLOC-1 remodel endosomal membranes into tubules. J. Cell Biol. *221*, e202110132. https://doi.org/10.1083/jcb.202110132.
46. Zhu, Y., Li, S., Jaume, A., Jani, R.A., Delevoye, C., Raposo, G., and Marks, M.S. (2022). Type II phosphatidylinositol 4-kinases function sequentially in cargo delivery from early endosomes to melanosomes. J. Cell Biol. *221*, e202110114. https://doi.org/10.1083/jcb.202110114.
47. Dennis, M.K., Delevoye, C., Acosta-Ruiz, A., Hurbain, I., Romao, M., Hesketh, G.G., Goff, P.S., Sviderskaya, E.V., Bennett, D.C., Luzio, J.P., et al. (2016). BLOC-1 and BLOC-3 regulate VAMP7 cycling to and from melanosomes via distinct tubular transport carriers. J. Cell Biol. *214*, 293–308. https://doi.org/10.1083/jcb.201605090.
48. Theos, A.C., Tenza, D., Martina, J.A., Hurbain, I., Peden, A.A., Sviderskaya, E.V., Stewart, A., Robinson, M.S., Bennett, D.C., Cutler, D.F., et al. (2005). Functions of adaptor protein (AP)-3 and AP-1 in tyrosinase sorting from endosomes to melanosomes. Mol. Biol. Cell *16*, 5356–5372. https://doi.org/10.1091/mbc.e05-07-0626.

49. Nguyen, T., Novak, E.K., Kermani, M., Fluhr, J., Peters, L.L., Swank, R.T., and Wei, M.L. (2002). Melanosome morphologies in murine models of hermansky-pudlak syndrome reflect blocks in organelle development. J. Invest. Dermatol. *119*, 1156–1164. https://doi.org/10.1046/j.1523-1747.2002.19535.x.

50. Nguyen, T., and Wei, M.L. (2004). Characterization of melanosomes in murine Hermansky-Pudlak syndrome: mechanisms of hypopigmentation. J. Invest. Dermatol. *122*, 452–460. https://doi.org/10.1046/j.0022-202X.2004.22117.x.

51. Cheli, Y., Luciani, F., Khaled, M., Beuret, L., Bille, K., Gounon, P., Ortonne, J.P., Bertolotto, C., and Ballotti, R. (2009). alphaMSH} and Cyclic AMP elevating agents control melanosome pH through a protein kinase A-independent mechanism. J. Biol. Chem. *284*, 18699–18706. https://doi.org/10.1074/jbc.M109.005819.

52. Huizing, M., Sarangarajan, R., Strovel, E., Zhao, Y., Gahl, W.A., and Boissy, R.E. (2001). AP-3 mediates tyrosinase but not TRP-1 trafficking in human melanocytes. Mol. Biol. Cell *12*, 2075–2085. https://doi.org/10.1091/mbc.12.7.2075.

53. Chen, J.W., Murphy, T.L., Willingham, M.C., Pastan, I., and August, J.T. (1985). Identification of two lysosomal membrane glycoproteins. J. Cell Biol. *101*, 85–95. https://doi.org/10.1083/jcb.101.1.85.

54. Luzio, J.P., Hackmann, Y., Dieckmann, N.M.G., and Griffiths, G.M. (2014). The biogenesis of lysosomes and lysosome-related organelles. Cold Spring Harb. Perspect. Biol. *6*, a016840. https://doi.org/10.1101/cshperspect.a016840.

55. Shearer, L.J., and Petersen, N.O. (2019). Distribution and co-localization of endosome markers in cells. Heliyon *5*, e02375. https://doi.org/10.1016/j.heliyon.2019.e02375.

56. Bissig, C., Hurbain, I., Raposo, G., and van Niel, G. (2017). PIKfyve activity regulates reformation of terminal storage lysosomes from endolysosomes. Traffic *18*, 747–757. https://doi.org/10.1111/tra.12525.

57. Humphries, W.H.t., Szymanski, C.J., and Payne, C.K. (2011). Endo-lysosomal vesicles positive for Rab7 and LAMP1 are terminal vesicles for the transport of dextran. PLOS One *6*, e26626. https://doi.org/10.1371/journal.pone.0026626.

58. Seiji, M., Fitzpatrick, T.B., and Birbeck, M.S. (1961). The melanosome: a distinctive subcellular particle of mammalian melanocytes and the site of melanogenesis. J. Invest. Dermatol. *36*, 243–252. https://doi.org/10.1038/jid.1961.42.

59. Halaban, R., Patton, R.S., Cheng, E., Svedine, S., Trombetta, E.S., Wahl, M.L., Ariyan, S., and Hebert, D.N. (2002). Abnormal acidification of melanoma cells induces tyrosinase retention in the early secretory pathway. J. Biol. Chem. *277*, 14821–14828. https://doi.org/10.1074/jbc.M111497200.

60. Erent, M., Meli, A., Moisoi, N., Babich, V., Hannah, M.J., Skehel, P., Knipe, L., Zupancic, G., Ogden, D., and Carter, T. (2007). Rate, extent and concentration dependence of histamine-evoked Weibel-Palade body exocytosis determined from individual fusion events in human endothelial cells. J. Physiol. *583*, 195–212. https://doi.org/10.1113/jphysiol.2007.132993.

61. Kneen, M., Farinas, J., Li, Y., and Verkman, A.S. (1998). Green fluorescent protein as a noninvasive intracellular pH indicator. Biophys. J. *74*, 1591–1599. https://doi.org/10.1016/S0006-3495(98)77870-1.

62. Decker, R.S., Decker, M.L., Thomas, V., and Fuseler, J.W. (1985). Responses of cultured cardiac myocytes to lysosomotropic compounds and methylated amino acids. J. Cell Sci. *74*, 119–135. https://doi.org/10.1242/jcs.74.1.119.

63. Johnson, D.E., Ostrowski, P., Jaumouillé, V., and Grinstein, S. (2016). The position of lysosomes within the cell determines their luminal pH. J. Cell Biol. *212*, 677–692. https://doi.org/10.1083/jcb.201507112.

64. Bright, N.A., Davis, L.J., and Luzio, J.P. (2016). Endolysosomes are the principal intracellular sites of acid hydrolase activity. Curr. Biol. *26*, 2233–2245. https://doi.org/10.1016/j.cub.2016.06.046.

65. Bartölke, R., Heinisch, J.J., Wieczorek, H., and Vitavska, O. (2014). Proton-associated sucrose transport of mammalian solute carrier family 45: an analysis in Saccharomyces cerevisiae. Biochem. J. *464*, 193–201. https://doi.org/10.1042/BJ20140572.

66. Sitaram, A., Piccirillo, R., Palmisano, I., Harper, D.C., Dell'Angelica, E.C., Schiaffino, M.V., and Marks, M.S. (2009). Localization to mature melanosomes by virtue of cytoplasmic dileucine motifs is required for human OCA2 function. Mol. Biol. Cell *20*, 1464–1477. https://doi.org/10.1091/mbc.e08-07-0710.

67. Seberg, H.E., Van Otterloo, E., Loftus, S.K., Liu, H., Bonde, G., Sompallae, R., Gildea, D.E., Santana, J.F., Manak, J.R., Pavan, W.J., et al. (2017). TFAP2 paralogs regulate melanocyte differentiation in parallel with MITF. PLOS Genet. *13*, e1006636. https://doi.org/10.1371/journal.pgen.1006636.

68. Visser, M., Kayser, M., and Palstra, R.J. (2012). HERC2 rs12913832 modulates human pigmentation by attenuating chromatin-loop formation between a long-range enhancer and the OCA2 promoter. Genome Res. *22*, 446–455. https://doi.org/10.1101/gr.128652.111.

69. Newton, R.A., Cook, A.L., Roberts, D.W., Leonard, J.H., and Sturm, R.A. (2007). Post-transcriptional regulation of melanin biosynthetic enzymes by cAMP and resveratrol in human melanocytes. J. Invest. Dermatol. *127*, 2216–2227. https://doi.org/10.1038/sj.jid.5700840.

70. Ancans, J., Hoogduijn, M.J., and Thody, A.J. (2001). Melanosomal pH, pink locus protein and their roles in melanogenesis. J. Invest. Dermatol. *117*, 158–159. https://doi.org/10.1046/j.0022-202x.2001.01397.x.

71. Ancans, J., and Thody, A.J. (2000). Activation of melanogenesis by vacuolar type H(+)-ATPase inhibitors in amelanotic, tyrosinase positive human and mouse melanoma cells. FEBS Lett. *478*, 57–60. https://doi.org/10.1016/s0014-5793(00)01795-6.

72. Chen, K., Minwalla, L., Ni, L., and Orlow, S.J. (2004). Correction of defective early tyrosinase processing by bafilomycin A1 and monensin in pink-eyed dilution melanocytes. Pigment Cell Res. *17*, 36–42. https://doi.org/10.1046/j.1600-0749.2003.00106.x.

73. Dooley, C.M., Schwarz, H., Mueller, K.P., Mongera, A., Konantz, M., Neuhauss, S.C.F., Nüsslein-Volhard, C., and Geisler, R. (2013). Slc45a2 and V-ATPase are regulators of melanosomal pH homeostasis in zebrafish, providing a mechanism for human pigment evolution and disease. Pigment Cell Melanoma Res. *26*, 205–217. https://doi.org/10.1111/pcmr.12053.

74. Ni-Komatsu, L., and Orlow, S.J. (2006). Heterologous expression of tyrosinase recapitulates the misprocessing and mistrafficking in oculocutaneous albinism type 2: effects of altering intracellular pH and pink-eyed dilution gene expression. Exp. Eye Res. *82*, 519–528. https://doi.org/10.1016/j.exer.2005.08.013.

75. Ito, M., Hashimoto, K., and Organisciak, D.T. (1982). Ultrastructural, histochemical, and biochemical studies of the melanin metabolism in eye and skin of pallid mice. J. Invest. Dermatol. *78*, 414–424. https://doi.org/10.1111/1523-1747.ep12507677.

76. Zhang, Q., Li, W., Novak, E.K., Karim, A., Mishra, V.S., Kingsmore, S.F., Roe, B.A., Suzuki, T., and Swank, R.T. (2002). The gene for the muted (mu) mouse, a model for Hermansky-Pudlak syndrome, defines a novel protein which regulates vesicle trafficking. Hum. Mol. Genet. *11*, 697–706. https://doi.org/10.1093/hmg/11.6.697.

77. Gautam, R., Novak, E.K., Tan, J., Wakamatsu, K., Ito, S., and Swank, R.T. (2006). Interaction of Hermansky-Pudlak syndrome genes in the regulation of lysosome-related organelles. Traffic *7*, 779–792. https://doi.org/10.1111/j.1600-0854.2006.00431.x.

78. Bennett, D.C., Cooper, P.J., Dexter, T.J., Devlin, L.M., Heasman, J., and Nester, B. (1989). Cloned mouse melanocyte lines carrying the germline mutations albino and brown: complementation in culture. Development *105*, 379–385. https://doi.org/10.1242/dev.105.2.379.

79. Bouchard, B., Fuller, B.B., Vijayasaradhi, S., and Houghton, A.N. (1989). Induction of pigmentation in mouse fibroblasts by expression of human

tyrosinase cDNA. J. Exp. Med. *169*, 2029–2042. https://doi.org/10.1084/jem.169.6.2029.

80. Winder, A.J. (1991). Expression of a mouse tyrosinase cDNA in 3T3 Swiss mouse fibroblasts. Biochem. Biophys. Res. Commun. *178*, 739–745. https://doi.org/10.1016/0006-291x(91)90170-c.
81. Calvo, P.A., Frank, D.W., Bieler, B.M., Berson, J.F., and Marks, M.S. (1999). A cytoplasmic sequence in human tyrosinase defines a second class of di-leucine-based sorting signals for late endosomal and lysosomal delivery. J. Biol. Chem. *274*, 12780–12789. https://doi.org/10.1074/jbc.274.18.12780.
82. Jimbow, K., Ishida, O., Ito, S., Hori, Y., Witkop, C.J., Jr., and King, R.A. (1983). Combined chemical and electron microscopic studies of pheomelanosomes in human red hair. J. Invest. Dermatol. *81*, 506–511. https://doi.org/10.1111/1523-1747.ep12522838.
83. Moyer, F.H. (1966). Genetic variations in the fine structure and ontogeny of mouse melanin granules. Am. Zool. *6*, 43–66. https://doi.org/10.1093/icb/6.1.43.
84. Liu, Y., Hong, L., Wakamatsu, K., Ito, S., Adhyaru, B., Cheng, C.Y., Bowers, C.R., and Simon, J.D. (2005). Comparison of structural and chemical properties of black and red human hair melanosomes. Photochem. Photobiol. *81*, 135–144. https://doi.org/10.1562/2004-08-03-RA-259.1.
85. Garcia, R.I., and Szabo, G. (1983). Modulation of melanosome ultrastructure in cultured embryonic pigment cells. J. Exp. Zool. *225*, 285–291. https://doi.org/10.1002/jez.1402250211.
86. Cook, A.L., Chen, W., Thurber, A.E., Smit, D.J., Smith, A.G., Bladen, T.G., Brown, D.L., Duffy, D.L., Pastorino, L., Bianchi-Scarra, G., et al. (2009). Analysis of cultured human melanocytes based on polymorphisms within the SLC45A2/MATP, SLC24A5/NCKX5, and OCA2/P loci. J. Invest. Dermatol. *129*, 392–405. https://doi.org/10.1038/jid.2008.211.
87. Iozumi, K., Hoganson, G.E., Pennella, R., Everett, M.A., and Fuller, B.B. (1993). Role of tyrosinase as the determinant of pigmentation in cultured human melanocytes. J. Invest. Dermatol. *100*, 806–811. https://doi.org/10.1111/1523-1747.ep12476630.
88. Halaban, R., Pomerantz, S.H., Marshall, S., Lambert, D.T., and Lerner, A.B. (1983). Regulation of tyrosinase in human melanocytes grown in culture. J. Cell Biol. *97*, 480–488. https://doi.org/10.1083/jcb.97.2.480.
89. Ostojić, J., Yoon, Y.S., Sonntag, T., Nguyen, B., Vaughan, J.M., Shokhirev, M., and Montminy, M. (2021). Transcriptional co-activator regulates melanocyte differentiation and oncogenesis by integrating cAMP and MAPK/ERK pathways. Cell Rep. *35*, 109136. https://doi.org/10.1016/j.celrep.2021.109136.
90. Bennett, D.C., Cooper, P.J., and Hart, I.R. (1987). A line of non-tumorigenic mouse melanocytes, syngeneic with the B16 melanoma and requiring a tumour promoter for growth. Int. J. Cancer *39*, 414–418. https://doi.org/10.1002/ijc.2910390324.
91. Sviderskaya, E.V., Hill, S.P., Evans-Whipp, T.J., Chin, L., Orlow, S.J., Easty, D.J., Cheong, S.C., Beach, D., DePinho, R.A., and Bennett, D.C. (2002). p16(Ink4a) in melanocyte senescence and differentiation. J. Natl. Cancer Inst. *94*, 446–454. https://doi.org/10.1093/jnci/94.6.446.
92. Oancea, E., Vriens, J., Brauchi, S., Jun, J., Splawski, I., and Clapham, D.E. (2009). TRPM1 forms ion channels associated with melanin content in melanocytes. Sci. Signal. *2*, ra21. https://doi.org/10.1126/scisignal.2000146.
93. Berson, J.F., Frank, D.W., Calvo, P.A., Bieler, B.M., and Marks, M.S. (2000). A common temperature-sensitive allelic form of human tyrosinase is retained in the endoplasmic reticulum at the nonpermissive temperature. J. Biol. Chem. *275*, 12281–12289. https://doi.org/10.1074/jbc.275.16.12281.
94. Berson, J.F., Harper, D.C., Tenza, D., Raposo, G., and Marks, M.S. (2001). Pmel17 initiates premelanosome morphogenesis within multivesicular bodies. Mol. Biol. Cell *12*, 3451–3464. https://doi.org/10.1091/mbc.12.11.3451.
95. Taylor, S.C., Rosselli-Murai, L.K., Crobeddu, B., and Plante, I. (2022). A critical path to producing high quality, reproducible data from quantitative western blot experiments. Sci. Rep. *12*, 17599. https://doi.org/10.1038/s41598-022-22294-x.
96. Hellemans, J., Mortier, G., De Paepe, A., Speleman, F., and Vandesompele, J. (2007). qBase relative quantification framework and software for management and automated analysis of real-time quantitative PCR data. Genome Biol. *8*, R19. https://doi.org/10.1186/gb-2007-8-2-r19.
97. Taylor, S.C., Nadeau, K., Abbasi, M., Lachance, C., Nguyen, M., and Fenrich, J. (2019). The ultimate qPCR experiment: producing publication quality, reproducible data the first time. Trends Biotechnol. *37*, 761–774. https://doi.org/10.1016/j.tibtech.2018.12.002.
98. Thomson, T.M., Mattes, M.J., Roux, L., Old, L.J., and Lloyd, K.O. (1985). Pigmentation-associated glycoprotein of human melanomas and melanocytes: definition with a mouse monoclonal antibody. J. Invest. Dermatol. *85*, 169–174. https://doi.org/10.1111/1523-1747.ep12276608.
99. Reynolds, E.S. (1963). The use of lead citrate at high pH as an electron-opaque stain in electron microscopy. J. Cell Biol. *17*, 208–212. https://doi.org/10.1083/jcb.17.1.208.
100. Tompkins, L.S., Nullmeyer, K.D., Murphy, S.M., Weber, C.S., and Lynch, R.M. (2002). Regulation of secretory granule pH in insulin-secreting cells. Am. J. Physiol. Cell Physiol. *283*, C429–C437. https://doi.org/10.1152/ajpcell.01066.2000.
101. Meli, A., McCormack, A., Conte, I., Chen, Q., Streetley, J., Rose, M.L., Bierings, R., Hannah, M.J., Molloy, J.E., Rosenthal, P.B., et al. (2023). Altered storage and function of von Willebrand Factor in human cardiac microvascular endothelial cells isolated from recipient transplant hearts. Int. J. Mol. Sci. *24*, 4553. https://doi.org/10.3390/ijms24054553.

Please cite this article in press as: Goff et al., Reprogramming of endolysosomes for melanogenesis in BLOC-1-deficient melanocytes, Current Biology (2025), https://doi.org/10.1016/j.cub.2025.06.031

STAR★METHODS

KEY RESOURCES TABLE

REAGENT or RESOURCE	SOURCE	IDENTIFIER
Antibodies		
HA tag	Abcam	Cat. # ab9110; RRID:AB_307019
TYRP1	ATCC	Cat. # TA99/Mel-5
LAMP2	Developmental Studies Hybridoma Bank	Cat. # GL2A7; RRID:AB_2314734
Goat anti-mouse AlexaFluor488	Invitrogen	Cat. # A-11001; RRID:AB_2534069
Goat anti-rabbit AlexaFluor568	Invitrogen	Cat. # A-11011; RRID:AB_143157
Goat anti-rat AlexaFluor568	Invitrogen	Cat. # A-11077; RRID:AB_141874
αPep7h (anti-TYR)	Marks lab	N/A
αPep13h (anti-PMEL)	Marks lab	N/A
TYRP1	Santa Cruz Biotechnology	Cat. # sc-166857; RRID:AB_2211147
Actin	Sigma-Aldrich	Cat. # A5060; RRID:AB_476738
γ-tubulin	Sigma	Cat. # T6557; RRID:AB_477584
Goat anti-mouse IgG-IRDye 800CW	Li-Cor	Cat. # 926-32210; RRID:AB_621842
Goat anti-Rabbit IgG-IR Dye 680R	Li-Cor	Cat. # 926-68071; RRID:AB_10956166
Donkey anti-mouse IgG (H+L) AlexaFluor790	Jackson ImmunoResearch	Cat. # 715-655-151; RRID:AB_2340871
Donkey anti-rabbit IgG (H+L) AlexaFluor680	Jackson ImmunoResearch	Cat. # 711-625-152; RRID:AB_2340627
Chemicals, peptides, and recombinant proteins		
12-0-tetradecanoyl phorbol acetate (TPA)	Sigma-Aldrich	Cat. # P8139
4-Norleucine,7-D-phenylalanine-alpha-melanocyte-stimulating hormone (NDP-MSH)	Sigma-Aldrich	Cat. # M8764
Forskolin	Sigma-Aldrich	Cat. # F6886
Cholera toxin	Sigma-Aldrich	Cat. # C8052
Bafilomycin A1	Sigma-Aldrich	Cat. # B1793
Cycloheximide	Sigma-Aldrich	Cat. # C1988-1G
L-Methionine methyl ester hydrochloride	Thermo Scientific Chemicals	Cat. # A15952.14
Monensin	Sigma-Aldrich	Cat. # M5273
Nigericin	Sigma-Aldrich	Cat. # N7143
Sodium cacodylate	Sigma-Alrich	Cat. # C0250
Osmium Tetroxide	Agar Scientific	Cat. # AGR1019
Propylene oxide	Sigma-Aldrich	Cat. # 82320
Agar 100 Resin Kit	Agar Scientific	Cat. # AGR1031
Uranyl acetate	Agar Scientific	Cat. # AGR1260A
Lead citrate	Agar Scientific	Cat. # AGR1210
Dodecenyl succinic anhydride	Agar Scientific	Cat. #R1053
Methyl nadic anhydride	Agar Scientific	Cat. #R1083
Benzyl dimethylamine	Agar Scientific	Cat. #AGR1062
Potassium ferricyanide	Sigma-Aldrich	Cat. # 702587
Tannic acid	TAAB Laboratories Equipment Limited	Cat. # T046
Sodium sulphate	Sigma-Aldrich	Cat. # 239313
TAAB 812 Resin kit	TAAB Laboratories Equipment Limited	Cat. # T024/1
Lipofectamine 3000	ThermoFisher Scientific	Cat. #L3000015
Critical commercial assays		
RNeasy Plus Mini Kit	Qiagen	Cat. # 74134
LunaScript RT SuperMix Kit	New England Biolabs	Cat. # M3010

(*Continued on next page*)

Please cite this article in press as: Goff et al., Reprogramming of endolysosomes for melanogenesis in BLOC-1-deficient melanocytes, Current Biology (2025), https://doi.org/10.1016/j.cub.2025.06.031

Continued

REAGENT or RESOURCE	SOURCE	IDENTIFIER
Luna Universal qPCR Master Mix	New England Biolabs	Cat. # M3003
Experimental models: Cell lines		
melan-pa: *Bloc1S6*$^{pa/pa}$	Functional Genomics Cell Bank at City St. George's University of London	N/A
melan-mu: *Bloc1S5*$^{mu/mu}$	Functional Genomics Cell Bank at City St. George's University of London	N/A
melan-a: *a/a*	Functional Genomics Cell Bank at City St. George's University of London	N/A
melan-Ink4a-Arf1: *Ink4a-Arf*$^{-/-}$	Functional Genomics Cell Bank at City St. George's University of London	N/A
melan-c2: *Tyr*$^{c\text{-}2J}$/*Tyr*$^{c\text{-}2J}$	Functional Genomics Cell Bank at City St. George's University of London	N/A
melan-mu:MuHA	Functional Genomics Cell Bank at City St. George's University of London	N/A
Oligonucleotides		
TYR Fwd: 5 ' CGA TGG AAC ACC TGA GGG AC	Integrated DNA Technologies	N/A
TYR Rev:5 ' AGT GGA CTG GCA AAT CCT TCC	Integrated DNA Technologies	N/A
Atp5b primer set (Anchor nucelotide: 115)	Primer Design Ltd.	geNorm kit (Discontinued)
Ubc primer set (Anchor nucelotide: 2627)	Primer Design Ltd.	geNorm kit (Discontinued)
B2m primer set (Anchor nucelotide: 202)	Primer Design Ltd.	geNorm kit (Discontinued)
Sdha primer set (Anchor nucelotide: 2018)	Primer Design Ltd.	geNorm kit (Discontinued)
Recombinant DNA		
pCR3/OCA2-HA	Michael Marks	N/A
pCI-HA-SLC45A2	Michael Marks	N/A
pN1-LAMP1-tdTomato	Tom Carter	N/A
Software and algorithms		
GraphPad Prism (version 10.2.1)	GraphPad	https://www.graphpad.com/
ImageJ	NIH	https://imagej.nih.gov/ij/
Photoshop CS6 (Version 13.0)	Adobe Systems	N/A
NIS Elements (Version 4.2)	Nikon	N/A
Image Studio (Version 5.2)	Li-Cor	N/A
AMT Capture Engine software (Version V602.580.20d)	Advanced Microscopy Techniques	N/A
Other		
RPMI-1640 Medium	Sigma-Alrich	Cat. # R7509
Fetal Bovine Serum	Gibco	Cat. # 10270106
Dextran, Oregon Green 488; 10,000 MW	Invitrogen	Cat. # D7170
L-Glutamine	Gibco	Cat. # 25030081
Penicillin-Streptomycin (10,000 U/mL)	Gibco	Cat. # 15140122
HEPES	Gibco	Cat. # 15630056
Protease Inhibitor cocktail	Roche	Cat. # 11697498001
Immobilon-FL PVDF Membrane	Millipore	Cat. # IPFL85R
Nitrocellulose membrane, 0.45 μm	BioRad	Cat. # 1620115
CitiFluor AF1 mounting solution	Agar Scientific	Cat. # AGR1320
Copper mesh grids	Agar Scientific	Cat. # AGG2415C
35 mm Dish with No. 1.5 Gridded Coverslip, 14 mm Glass Diameter	MatTek	Cat. # P35G-1.5-14-C-GRD
CitiFluor AF1 mounting solution	Agar Scientific	Cat. #AGR1320
Black 96 well plate	Greiner Bio-One	Cat. #655900

Please cite this article in press as: Goff et al., Reprogramming of endolysosomes for melanogenesis in BLOC-1-deficient melanocytes, Current Biology (2025), https://doi.org/10.1016/j.cub.2025.06.031

EXPERIMENTAL MODEL AND STUDY PARTICIPANT DETAILS

BLOC-1-deficient murine melanocytes, melan-pa and melan-mu[35] from Pallid (B6.Cg-*Bloc1s6*^{pa}/J) and Muted (B6C3 *A*$^{w-J}$/*A-Bloc1s5*^{mu}/J) mice respectively, wild type melan-a[90] from C57BL/6 mice and melan-Ink4a-Arf1[91] from C57BL/6-*Ink4a-Arf*$^{-/-}$ mice, BLOC-1-rescued (melan-mu:MuHA),[35] and the albino line melan-c2 from C57BL/6-*Tyr*$^{c/c}$ mice (unpublished) have been described. The sex of the newborn mice from which these lines were derived was not noted at the time of establishment. Cells were maintained in RPMI 1640 media supplemented with 2 mM L-glutamine, 10,000 units/ml penicillin, 100 μg/ml streptomycin sulphate, 10% fetal bovine serum, and 200 nM 12-0-tetradecanoyl phorbol acetate (TPA) along with and either 200 pM cholera toxin (CT), 100 pM 4-Norleucine,7-D-phenylalanine-alpha-melanocyte-stimulating hormone (NDP-MSH), or 20 μM forskolin for 7 days unless otherwise stated. For cycloheximide chase experiments cells were cultured with or without 20 μM forskolin for 7 days and then treated with 25 μg/ml cycloheximide, 20 nM bafilomycin A1 (BafA1), or both for 0, 2, 4 and 8 hrs; an equal volume of vehicle (DMSO) was added to controls. For treatment with deacidification agents, BLOC-1-deficient melanocytes were cultured with or without 20 μM forskolin for 6 days before the medium was changed to contain 20 mM HEPES with or without 20 μM forskolin, 10 mM methionine methyl ester (MME), and/or 20 nM BafA1. Based on preliminary survival curves, cells were treated for 24 hours with MME or 6 hours with BafA1 before harvesting samples to quantify the melanin content as described.

METHOD DETAILS

Intracellular melanin content

Murine melanocytes were plated at 1 x 10^4 cells/ml into 35 mm (pigmented melanocytes) or 10 cm dishes (BLOC-1-deficient/albino melanocytes) and treated as described above under Experimental model and study participant details. Melanin content was quantified based on a method previously described.[92] Briefly, cells were harvested and resuspended in culture medium with an aliquot taken for determination of cell number. The remaining cells were centrifuged at 16,200 x g for 15 minutes at 4°C with the supernatant removed. The cells were lysed with 1% v/v Triton X-100 in complete phosphate-buffered saline lacking calcium and magnesium (PBSA) for 30 minutes at 4°C. The lysate was centrifuged at 16,200 x g for 30 minutes at 4°C. The insoluble fraction containing the melanin was resuspended in 1M NaOH/10% v/v DMSO and incubated at 85°C for at least 30 minutes or until the melanin was fully dissolved. The solubilized melanin was read against a blank of 1M NaOH/10 % v/v DMSO at 405 nm in a SpectraMax 340 spectrophotometer (Molecular Devices). The absorbance was compared to a standard curve of absorbance of known concentrations of synthetic melanin to determine melanin content. The melanin concentration was normalized to the total cell number of each replicate with the background absorbance values of the unpigmented melanocyte line, melan-c2, subtracted (see Figure S1).

Western blotting and quantification

Cells were cultured in 10 cm dishes with or without cAMP elevating agents as described above. After 7 days in culture, medium was removed, dishes were placed on ice and washed with ice-cold PBSA. Cells were lysed with 500 μl of ice-cold lysis buffer (50 mM Tris pH 8.0, 150 mM NaCl, 2 mM EDTA, 1% v/v Triton-X 100, 1% w/v sodium dodecyl sulphate (SDS)) containing complete protease inhibitor (Roche), and the lysate was homogenized using a 21-gauge needle and clarified by centrifugation at 16,200 x g for 15 minutes at 4°C. Total protein concentration was determined before separation by SDS-PAGE and transferred to a polyvinylidene difluoride (PVDF)-FL (Millipore) or reinforced nitrocellulose (Bio-Rad) membrane. The membrane was incubated with primary antibodies [αPep7h, against the C-terminus of human TYR[93]; αPep13h against the C-terminus of human PMEL[94]; TYRP1 (G-9, Santa Cruz Biotechnology sc-166857); anti-actin (Sigma-Aldrich (A5060) and anti-γ-tubulin (Sigma, Cat. #T6557)] overnight diluted in 5% non-fat milk in TBS-T (20 mM Tris, 137 mM sodium chloride, 0.1% or 0.2% v/v Tween-20, pH 7.6). Blots were washed three times in TBS-T, then incubated with fluorescently-labelled secondary antibodies [IRDye 800CW Goat anti-Mouse IgG (Li-Cor, 926-32210), IR Dye 680RD Goat anti-Rabbit IgG (Li-Cor, 926-68071) Alexa Fluor 680- and 790-conjugated AffiniPure donkey anti-mouse IgG (H + L; Jackson Immunoresearch, Cat. #715-655-151) and anti-rabbit IgG (H + L; Jackson Immunoresearch Cat. #711-625-152)] diluted in 5% non-fat milk in TBS-T before washing three times and signal detection using the LiCor Odyssey Clx (Li-Cor Biosciences). To quantify changes in protein expression between samples, densitometric analysis was performed using Image Studio (Version 5.2, Li-Cor) or Fiji-ImageJ (National Institutes of Health). The fluorescent intensities of each band were measured and the background values subtracted. Relative protein expression was determined using a method previously described.[95] Briefly the ratio of signal of interest to the signal of the loading control was calculated for each replicate (IS/LCS). This was then averaged for the untreated control only (mean IS/LCS). The normalized ratio of each individual value for each experimental condition was normalized to the untreated control by dividing the IS/LCS for each condition by the mean IS/LCS of the untreated control (normalized IS/LCS ratio). The mean of the normalized IS/LCS ratios for each experimental condition were determined and are shown in the figures. Images were further processed using Fiji-ImageJ and/or Adobe Photoshop CS6 Version 13.0 (Adobe Systems).

Cycloheximide chase assay

Cells were cultured as described above. Cells were detached by incubation for 10-15 min in PBSA/ 10 mM EDTA and collected by centrifugation at 500 × *g* for 5 min. Cell pellets were washed with ice cold PBSA/0.1% FBS, and whole cell lysates were prepared by resuspending in cold 50 mM Tris-HCl/ pH 7.4, 2 mM EDTA/, 150 mM NaCl, 1 mM DTT, and 1× protease inhibitor cocktail (Roche) and

Please cite this article in press as: Goff et al., Reprogramming of endolysosomes for melanogenesis in BLOC-1-deficient melanocytes, Current Biology (2025), https://doi.org/10.1016/j.cub.2025.06.031

sonicating on ice using the Sonic Dismembrator Model 100 (Thermo Fisher Scientific). Cell extracts were cleared by centrifugation at 13,000 x *g* at 4°C for 15 min and the supernatants were collected. Concentrated Laemmli sample buffer with 2-mercaptoethanol was added to cell lysates and heated at 95–100°C for 10 min. Samples were then fractionated by SDS-PAGE on 10% polyacrylamide gels, transferred to nitrocellulose membranes (BioRad), and immunoblotted as described above.

Quantitative Reverse Transcription Polymerase Chain Reaction (RT-qPCR)

Melanocytes were plated at 3 x 10^4 cells/ml and treated with cAMP elevating agents as described above. Cells were harvested by trypsinization and centrifugation at 300 x g for 5 minutes at 4°C. RNA was extracted from the cell pellets using the RNeasy Plus Mini kit (Qiagen) as per the manufacturer's instructions. Between 0.5-1 μg of each RNA sample was reverse transcribed into cDNA using the LunaScript RT SuperMix Kit (New England Biolabs Inc.) as per the manufacturer's instructions. Primers were designed for *Tyr* (Accession number NM_011661.5) using Primer-BLAST and were ordered from Integrated DNA Technologies (see key resources table for primer information). Primer efficiency and suitability were tested and the most stable reference genes were identified for each cell line using a geNorm gene kit (Primer Design, UK). The optimal reference genes and number required for normalization were determined by GeNorm analysis[96] [melan-a: ATP synthase, H+ transporting mitochondrial F1 complex, beta subunit (*Atp5b*) and ubiquitin C (*Ubc*); melan-pa: β-2microglobulin (*B2m*) and *Ubc*; melan-mu:MuHA and melan-mu: *B2m* and succinate dehydrogenase complex, subunit A (*Sdha*)]. Amplification was carried out in a clear, low-profile 96-well plate (Thermo Fisher Scientific) and sealed with optically clear film (Thermo Fisher Scientific). Each well contained 20 μl of reaction mix as follows: 2 μl cDNA [diluted 1 in 10 in RNase free water (Gibco)], 2 μl each of forward primer and reverse primer, 10 μl of Luna Universal qPCR Master Mix (New England Biolabs), and 4 μl RNase free water. Where appropriate the cDNA was replaced with the no template control sample or the no reverse transcriptase samples. The plate was centrifuged for 1 minute at 300 x g and RT-PCR was carried out on a CFX Connect Real-Time PCR Detection System (Bio-Rad) with the following amplification parameters:

1. Initial denaturation: 95°C, 60 seconds
2. Denaturation: 95°C, 15 seconds
3. Extension'; 60°C, 30 seconds (including plate read)
4. Steps 2 and 3 were repeated a further 44 times
5. Melt curve: 60-95°C

To determine relative gene expression, a previously described method was used.[97] Briefly, the mean quantitative cycle (Cq) values of the gene of interest (GOI) and the reference genes for the untreated control were calculated. The relative difference in Cq values (ΔCq) between the mean Cq values for the untreated control GOI and reference genes, and the for the GOI and reference genes for each individual experimental condition was determined. Relative quantities (RQ) were determined using $2^{\Delta Cq}$ values. The normalization factor was determined by calculating the geometric mean of the RQ values. The relative normalized expression for the GOI was determined for each sample by dividing the individual RQ values by the normalization factor and is log-transformed ($\log_2$). These log-transformed values were using for statistical analysis. The mean normalized fold expression was calculated using the geometric mean of the relative normalized expression values for each experimental condition and these values were used for graphical representation of the data.

Immunolabelling, Immunofluorescence Microscopy and colocalization analysis

Melanocytes were plated onto glass coverslips at 3 x 10^4 cells/ml and treated with cAMP elevating agents as described above or transfected as described below. Cells were fixed for 20 minutes with 4% paraformaldehyde in PBSA, rinsed with PBSA and incubated for 5 minutes with 50 mM ammonium chloride. Permeabilization/blocking buffer (PSS: 0.05% v/v saponin, 2% v/v FBS in A) was added to the coverslips for 5 minutes at room temperature and then cells were labelled with primary antibodies (TA99/Mel-5 against TYRP1 (ATCC),[98] anti-HA tag (ab9110, Abcam) and GL2A7 against LAMP2 (Developmental Studies Hybridoma Bank, USA) prepared in PSS for 1 hour. Cells were then washed three times and incubated with fluorescently-conjugated secondary antibodies [AlexaFluor488 goat anti-mouse (Life Technologies), AlexaFluor568 goat anti-rabbit (Life Technologies) or AlexaFluor568 goat anti-rat (Life Technologies)] for 1 hour. The cells were washed 3 times with PSS and sometimes incubated with 1 μg/ml DAPI in the dark for 10 minutes. The cells were then washed 3 times with PBSA and twice with water before mounting onto microscope slides with CitiFluor AF1 mounting solution (Agar Scientific). The cells were imaged using a Nikon A1R inverted confocal microscope with NIS Elements software (Version 4.2; Nikon). Images were prepared for presentation using Adobe Photoshop CS6 Version 13.0 (Adobe Systems).

Object-based colocalization analysis between melanin and the relevant marker(s) for each experiment was measured using ImageJ as described.[47] Briefly, 8-bit, single channel images were opened in ImageJ. Bright field images of melanin were inverted with brightness and contrast manually adjusted. Single cells for analysis were chosen and isolated using the "ROI tool". The perinuclear region was removed from the analysis using the "ROI tool". For each channel, the background was removed, using the "Subtract Background" tool before manual thresholding to render the image binary (using the original image as a reference). This was repeated for each channel. Binary images of melanin were multiplied by the relevant marker using the "Image Calculator" tool. For analysis of melanin colocalization in compartments that were positive for two markers, the binary images of each marker

Please cite this article in press as: Goff et al., Reprogramming of endolysosomes for melanogenesis in BLOC-1-deficient melanocytes, Current Biology (2025), https://doi.org/10.1016/j.cub.2025.06.031

were multiplied together before multiplying the resulting image with the melanin channel. The percentage of melanin-occupying area colocalizing with each marker was determined relative to the total melanin-occupying area for each image.

Conventional transmission electron microscopy and quantification of pigmented organelles

BLOC-1-deficient melan-mu and BLOC-1^{R} melan-mu:MuHA melanocytes were plated at 3 x 10^4 cells/ml in 10 cm dishes and cultured with TPA in the presence or absence of forskolin as described above. The medium was removed, cells were washed in PBSA and fixed with 0.5% Karnovsky's fixative (0.5% w/v PFA, 72 mM sodium cacodylate, 4 mM calcium chloride, 2.5% w/v glutaraldehyde) for 1-2 hours. This was removed, replaced with 2% Karnovsky's fixative (2% w/v PFA, 72 mM sodium cacodylate, 4 mM calcium chloride, 2.5% w/v glutaraldehyde) and left overnight. The cells were harvested by scraping and centrifugation at 96 x g for 5 minutes, washed twice with 0.1 M sodium cacodylate for 15 minutes, and incubated with 2% w/v osmium tetroxide for 1 hour. Cells were washed twice for 15 minutes each with 0.1 M sodium cacodylate, dehydrated using an ethanol series (2 x 15 minutes in 70% ethanol, 2 x 15 minutes in 90% ethanol and 3 x 30 minutes in absolute ethanol) and then washed 3 times with propylene oxide for 10 minutes each. The samples were infiltrated for 1 hour with a 1:1 mix of propylene oxide and resin consisting of 36 g Agar 100 (Agar Scientific), 24 g dodecenylsuccinic anhydride (DDSA, Agar Scientific), 15 g methyl nadic anhydride (MNA, Agar Scientific) and 1.13 g of benzyl dimethylamine (BDMA, Agar Scientific). This was replaced with 100% resin and left for a further hour. The resin was replaced, and pellets were left to polymerize at 60°C for 48 hours.

Once polymerized, the block was trimmed and ultra-thin sections (approx. 90 nm) were taken using a UltraCutE ultramicrotome (Reichert/Leica) and transferred to copper mesh grids (Agar Scientific). The ultra-thin sections were post-stained by inverting the grids onto a drop of 2% v/v uranyl acetate for 10 minutes at room temperature in the dark followed by 5 X 30 second washes in dH2O. The grid was then placed onto a drop of Reynolds' lead citrate[99] for 90 seconds, washed 5 times for 30 seconds each in dH2O, and left to dry before imaging. Images were taken on a Hitachi TEM H-7100 with an AMT XR-16 camera using AMT Capture Engine software (Version V602.580.20d). The maximum length and width of individual melanosomes/melanin-containing organelles was measured from electron microscopy images using the AMT Capture Engine software (Version V602.580.20d). A minimum of 100 such organelles were counted for either melan-mu:MuHA (untreated or treated with forskolin) and melan-mu (untreated or treated with forskolin) from a minimum of 4 preparations each.

Correlative light and electron microscopy (CLEM)

BLOC-1-deficient melan-mu were plated at 1x10^4 cells/ml onto 35 mm dishes in which is attached a 1.5 thickness 14 mm diameter gridded coverslip with a raised alphanumeric pattern (MatTek Corporation, USA). Cells were cultured in the presence or absence of forskolin as described above for 7 days. Cells were then washed twice with PBSA prior to fixation with 4% w/v PFA and 0.025% v/v glutaraldehyde for 15 minutes at room temperature. The fixative was removed, and cells were immunolabelled for fluorescence microscopy using LAMP2 as described above, except that after incubation with the secondary antibody, the dishes were incubated with 1 μg/ml DAPI for 10 minutes in the dark and washed 3 times with PBSA for 5 minutes each. Dishes were left in PBSA for imaging.

Dishes were imaged on a Nikon A1R inverted confocal microscope with the NIS Elements software (Version 4.2). Regions of interest were imaged at 60 x magnification, noting the alphanumeric coordinates of these regions to locate the same region once cells had been embedded for electron microscopy. After confocal imaging, the cells were further fixed using Karnovsky's fixative as described above. Cells were then washed twice in 0.1 M sodium cacodylate for 5 minutes each and incubated with 1.5% w/v potassium ferricyanide and 1% osmium tetroxide (Agar Scientific) for 1 hour on ice. This was followed by 3 x 5-minute washes with 0.1 M sodium cacodylate and subsequent incubation with 1% w/v tannic acid (TAAB Laboratories Equipment Limited) for 45 minutes at room temperature. The cells were washed and incubated with 1% w/v sodium sulphate for 5 minutes prior to dehydration in an ethanol series as described above.

Following dehydration, cells were infiltrated for 1 hour with a 1:1 mix of absolute ethanol and resin composed of 12 g TAAB 812 resin (TAAB Laboratories Equipment Limited), 4.75 g DDSA (TAAB Laboratories Equipment Limited), 8.25 g MNA (TAAB Laboratories Equipment Limited) and 0.75 g of BDMA (TAAB Laboratories Equipment Limited). The resin was replaced with 100% resin for 2 hours before the resin was replaced and left for another 2 hours. The gridded coverslips attached to the dish were placed onto the bottom of a sawn-off 15ml tube containing resin before polymerization at 60°C for 48 hours.

Once polymerized, the dish was removed from the tube leaving the cells embedded in the resin along with the alphanumeric coordinates. The coordinates of regions of interest were identified on the polymerized resin surface prior to sectioning by Dr. Heather Brooks (Image Resource Facility, St. George's University of London). All sections were collected and placed on Formvar coated grids and post-stained as described above. Images were taken on a Hitachi TEM H-7100 with an AMT XR-16 camera using AMT Capture Engine software (Version V602.580.20d). Low magnification images were taken to identify the cell(s) of interest on the section and the orientation relative to the grid. Higher magnification images were taken for presentation. To correlate the light and electron microscopy images, an electron micrograph of an area of interest was chosen and the corresponding area within the light microscopy image was enlarged using Adobe Photoshop CS6, so the area/cell(s) were the same size as those in the electron microscopy image. These images were then correlated by identifying specific features (e.g., membrane protrusions, nucleus etc.) within both images and aligning them accordingly using Adobe Photoshop CS6. The light microscopy image was overlaid onto the electron micrograph using the 'Screen' function in Adobe Photoshop.

Please cite this article in press as: Goff et al., Reprogramming of endolysosomes for melanogenesis in BLOC-1-deficient melanocytes, Current Biology (2025), https://doi.org/10.1016/j.cub.2025.06.031

Transfection and quantification

BLOC-1-deficient melanocytes were cultured on glass coverslips without cAMP-elevating agents as described above. When cells were ~70% confluent they were transfected with 500 ng of either OCA2 (pCR3/OCA2-HA[66]) or SLC45A2 (pCI-HA-SLC45A2[12]) using Lipofectamine 3000 (ThermoFisher) as per the manufacturer's instructions. After 48 hours the cells were fixed and processed for IFM as described above. The identity of the cells and plasmids used on the coverslips was blinded before immunolabelling with anti-LAMP2, anti-HA tag and DAPI and confocal microscopy analysis as described above. In total at least 150 HA-tag positive cells were imaged for each transgene from at least 3 independent experiments and the percentage of HA-positive cells which were pigmented was quantified. Examples of the distinction between unpigmented and pigmented cells can be found in Figure S6A and is based on a similar analysis previously described.[12]

Lysosomal pH measurements

In vitro calibration curves were generated using the pH sensitive fluorophore Oregon Green conjugated to 10,000 MW dextran as previously described.[60,61] Briefly calibration buffers containing 120 mM KCl, 20 mM NaCl, 1 mM $MgSO_4$, 20 mM 4-(2-hydroxyethyl)-1-piperazineethanesulfonic acid (HEPES), 0.5 mM $CaCl_2$, and 10 mM glucose were adjusted to different pH values (pH 2 - 8). 50 μg/ml Oregon-Green Dextran (InvitroGen) was then diluted into each of these different pH buffers and transferred to a black-wall 96 well plate (Greiner Bio-One). The fluorescence intensity was measured on a BioTek Synergy LX multi-mode reader at room temperature. Calibration curves were generated by normalizing the fluorescence intensity of each pH value to the maximal fluorescence measured at pH 7 and curves were fitted using a four-parameter logistic model[100] using GraphPad Prism (Version 10.2.1). From this, the pKa and the Hill coefficient were calculated.

For *in vivo* calibration curves, melan-a cells were cultured in black-wall 96 well plates (Greiner Bio-One) for 6 days. The medium was removed, and cells were washed once with PBSA and incubated overnight with 250 μg/ml Oregon-Green Dextran (InVitroGen) in full growth medium. The next day the medium was removed and the cells were washed 3 times with PBSA and incubated with full growth medium for 2 hours to enable the fluorescently-labelled dextrans to reach terminal lysosomes. The medium was then removed, cells were washed twice with PBSA and then were incubated with calibration buffer at pH 7 (as described above). Baseline fluorescence intensity measurements were recorded using BioTek Synergy LX multi-mode reader at room temperature. The pH 7 calibration buffer was removed and replaced with calibration buffers at various pH values (pH 3.5 - 8.0; as described above) containing 5 μM nigericin and 5 μM monensin as previously described.[60] Fluorescence intensity was measured on a BioTek Synergy LX multi-mode reader at room temperature over 20 minutes to allow for equilibration. Calibration curves were generated as described above. To visualize Oregon-Green Dextran labelled lysosomes, BLOC-1-deficient melan-pa melanocytes were transiently transfected to express LAMP1-tdTomato (as described above) and subsequently exposed to Oregon Green-Dextran for 16 hours followed by a 2 hour chase period. Cells were then fixed and imaged by confocal microscopy as described above.

To measure the pH of lysosomes, melanocytes were first plated at 3 x 10^4 cells/ml in black-wall 96 well plates (Greiner Bio-One) in the presence or absence of CT, NDP-MSH or forskolin for 6 days. The medium was removed and cells were washed once with PBSA and then incubated overnight with 250 μg/ml Oregon-Green Dextran in full growth medium containing the relevant cAMP-elevating agent or vehicle. The next day the medium was removed and the cells were washed 3 times with PBSA and incubated with full growth medium for 2 hours to enable the fluorescently-labelled dextrans to reach terminal lysosomes. The medium was then removed and cells were washed twice with PBSA and then incubated with pH 7 calibration buffer (as described above). Baseline fluorescence intensity measurements were recorded using BioTek Synergy LX multi-mode reader at room temperature (5 reads with a 30 second interval between each) and then 2 M ammonium chloride was added to determine Fmax. The background fluorescent values of unlabeled cells in pH 7 calibration buffer were subtracted from both the steady-state and Fmax values and lysosomal pH was calculated using an equation previously described[60]:

$$pH = pKa - \left(\frac{1}{nH}\right)\cdot\log\left(\frac{Fmax}{F} - 1\right)$$

where *pKA* is pH corresponding to 50% fluorescent intensity, *nH* is the Hill coefficient (both derived from the in vivo calibration curve), *F*max is the maximum fluorescent intensity (minus background fluorescence) upon the addition of ammonium chloride, and *F* is the steady state fluorescent intensity (minus background fluorescence). The assay was validated by comparing the steady state lysosomal pH of untreated melanocytes with the lysosomal pH of melanocytes treated with the known lysosomal pH neutralizing agents BafA1 and MME (see Figure S5B).

To measure the pH of individual lysosomes, BLOC-1-deficient melan-mu melanocytes were plated at 3 x 10^4 cells/ml in 35 mm glass bottom dishes (VWR) in the presence or absence of 20 μM forskolin for 6 days. The cells were allowed to internalize Oregon-Green Dextran before a 2-hour chase as described above. The medium was then removed and cells were washed twice with PBSA and then incubated in pH 7 calibration buffer (without monensin or nigericin). Images were taken on an Olympus IX71 inverted fluorescence microscope using a U-Plan-Apo 100x 1.35 NA objective with a Ixon3 EMCCD camera (Andor). The EMCCD camera was operated in frame transfer mode at full gain and cooled to -70°C. 512 by 512 pixel images were acquired at 5 frames per second throughout the experiment. Epifluorescence measurements of Oregon-Green Dextran labeled lysosomes were acquired at steady-state and then immediately after exposure to 2 M ammonium chloride (to determine Fmax). The pH of individual lysosomes was derived from these epifluorescence measurements using a previously described macro in ImageJ[101] and the parameters describing the relationship between Oregon-Green fluorescence and pH from the calibration curves is shown in Figure S4A. The

Please cite this article in press as: Goff et al., Reprogramming of endolysosomes for melanogenesis in BLOC-1-deficient melanocytes, Current Biology (2025), https://doi.org/10.1016/j.cub.2025.06.031

pH of late endosomes/lysosomes was quantified by measuring the mean intensity of individual organelles from images generated in ImageJ as described above.

QUANTIFICATION AND STATISTICAL ANALYSIS

Statistical data are presented as mean or geometric mean ± SEM, except in Figures S3C, S3E, and S3G in which data are presented as mean ± SD. Statistics were calculated in GraphPad Prism (version 10.2.1) using one-way ANOVA with Dunnett's multiple comparison test or a post-hoc Tukey test, two-tailed student's t-test or two-way ANOVA with a post-hoc Tukey test as specified in the figure legends. A p value < 0.05 was considered as statistically significant.